1-1-2015

Synthesis, Characterization, and Mechanism Study of Carbon-Encapsulated Copper Nanoparticles

Weiqi Leng

Synthesis, characterization, and mechanism study of carbon-encapsulated copper nanoparticles

By

Weiqi Leng

A Dissertation
Submitted to the Faculty of
Mississippi State University
in Partial Fulfillment of the Requirements
for the Degree of Doctor of Philosophy
in Forest Resources
in the Department of Sustainable Bioproducts

Mississippi State, Mississippi

August 2015

Synthesis, characterization, and mechanism study of carbon-encapsulated copper nanoparticles

By

Weiqi Leng

Approved:

_____

H. Michael Barnes
(Major Professor)

_____

Jilei Zhang
(Co-Major Professor)

_____

El Barbary M. Hassan
(Committee Member)

_____

Dragica Jeremic Nikolic
(Committee Member)

_____

Abdolhamid Borazjani
(Committee Member)

_____

George M. Hopper
Dean
College of Forest Resources

Name: Weiqi Leng

Date of Degree: August 14, 2015

Institution: Mississippi State University

Major Field: Forest Resources

Major Professor: Drs. H. Michael Barnes, Jilei Zhang

Title of Study: Synthesis, characterization, and mechanism study of carbon-encapsulated copper nanoparticles

Pages in Study: 97

Candidate for Degree of Doctor of Philosophy

In this project, the synthesis of carbon encapsulated copper nanoparticles using sustainable bioproducts as raw material was systematically studied. The synthesis mechanism, process parameters, and functionalization of carbon encapsulated copper nanoparticles were well established.

In a preliminary study, carbon encapsulated copper nanoparticles were successfully synthesized at 1000 ºC, 1h, 20 ºC/min, and 1800 sccm argon gas flow rate using BCL-DI lignin as the carbon source. Carbon encapsulated copper nanoparticles were mainly located at defect sites. Copper was found not tightly encapsulated by graphene shells. The carbon encapsulated copper nanoparticles were uniformly distributed.

The conversion of copper ions into copper atoms occurred at above 300 ºC, with the company of decomposition of BCL-DI lignin into CO, CO_2, and hydrocarbon gases. The growth of graphene layers was proposed to start above 300 ºC. TEM images illustrated the onset of growth of graphene at the edge of the surface at 400 ºC, and the formation of graphene bands at 500 ºC. Copper catalyst continued to facilitate the

decomposition of lignin functional groups at 600 ºC. Further increasing the temperature retarded the degradation of lignin, while assisted the reconstruction of the defective sites of the graphene layers, producing higher quality products. Plastic film phase of lignin dominated on the synthesis of carbon encapsulated copper nanoparticles, while gaseous phase had little impact.

The orthogonal experiment revealed that temperature played the most important role in the growth of graphene: high temperature was preferred in order to obtain less defective sites. The optimum synthesis parameters were suggested as 1000 °C, 30 min duration time, 20 °C/min temperature rising ramp, and 1200 sccm argon gas flow rate. Post heat treatment was proved to be a feasible way to improve the crystallinity of graphite. Amorphous carbon was removed or converted into crystalline graphite under heat and oxygen.

FTIR spectra confirmed the covalent linkages between carbon encapsulated copper nanoparticles and N-methyl-2-pyrrolidone and polyvinylpyrrolidone, indicating a successful functionalization. This study has presented a homogeneous carbon encapsulated copper nanoparticles solution in water and ethanol, and paved ways for further functionalization of CECNs.

Key words: Graphene, synthesis, mechanism, functionalization

DEDICATION

I would like to dedicate this research to my mother, Yulan Wei, and my wife, Rui Sun.

ACKNOWLEDGEMENTS

I would first like to extend my sincere gratitude to my major professor, Dr. H. Michael Barnes, and co-advisor, Dr. Jilei Zhang, without their guidance and financial support I could not have finished this work. I would like to thank Drs. El Barbary Hassan, and Dragica Jeremic, my committee members, whom have both supported me on this endeavor with their expertise and encouragement, and gave me access to their labs and equipment. I would like to thank Dr. Zhiyong Cai, the project leader, for providing free experiment material and sharing information with me. A big thank you to Dr. Mojgan Nejad, Franklin Quin, Amy Rowlen, Qiangu Yan, Xuefeng Zhang, Bhawna Soni, Yan Luo, I-Wei Chu, Amanda Lawrence, Rooban Venkatesh K G Thirumalai, Yan Wang, Xiaoling Zhou, who helped me collect raw materials, make samples, and finish all experiments on time. I wish to thank Mississippi State University and the Department of Sustainable Bioproducts for the education provided to me, and the opportunity to further it. Thank you all.

TABLE OF CONTENTS

LIST OF TABLES

LIST OF FIGURES

NOMENCLATURE

BCL-DI	Deionized water purified BioChoice Lignin
CECNs	Carbon Encapsulated Copper Nanoparticles
TEM	Transmission Electron Microscope
SEM	Scanning Electron Microscope
FTIR-ATR	Fourier Transform Infrared Spectroscopy- Attenuated Total Reflectance
TGA	Thermogravimetric Analysis
I_D/I_G	Intensity ratio of D peak to G peak
CVD	Chemical Vapor Deposition
XRD	X-Ray Diffraction

CHAPTER I

INTRODUCTION

1.1 Background

Metal nanoparticles have been studied intensively due to their unique physical and electrical properties and widespread potential applications. However, the unique structure makes them unstable and easily oxidized and consequently, they lose the original preferred properties. These drawbacks have impeded the utilization of the metal nanoparticles. Encapsulation of metal nanoparticles by stable elements has been studied to conquer the drawbacks.

Graphene is a promising candidate to shield the metal nanoparticles. It is compatible with many materials, and it has electrical and mechanical properties which can improve the stability and kinetics of metal nanoparticles. In the meantime, graphene could preserve the pristine properties of metal nanoparticles.

In order to use graphene as a shield, two issues need to be addressed: what is the synthesis mechanism of carbon encapsulated metal nanoparticles and which parameters can and how to affect the yield and quality of graphene.

1.2 Literature review

1.2.1 Metal nanoparticles

Metal nanoparticles are particles between 1 and 100 nanometers in size. They have gained scientific interests due to a high surface to volume ratio and quantum-size effect (Obare and Meyer 2004). A large surface area is beneficial for functional groups attachment to the metal surface. With modification metal nanoparticles have promising potential application in biotechnological industry (Mody et al 2010). Metal nanoparticles can be produced through both physical and chemical pathways, of which, the chemical method is more popular. Metal ions can be reduced into metal atoms, followed by aggregation of metal atoms and formation of metal nanoparticles.

Metal nanoparticles should be stable in air during applications. However, due to the high surface to volume ratio, they are unstable and lose their original properties.

1.2.2 Graphene

Graphene is made of a single layer of carbon atoms that are bonded together with repeating C=C double bond. It can be considered to have a two dimensional configuration (Khenfouch et al 2014). The flat honeycomb pattern (Figure 1.1) grants graphene many unusual characteristics, including huge surface area, high mechanical strength, excellent electrical and thermal conductivity (Balandin et al 2008; Bolotin et al 2008; Lee et al 2008; Morozov et al 2008).

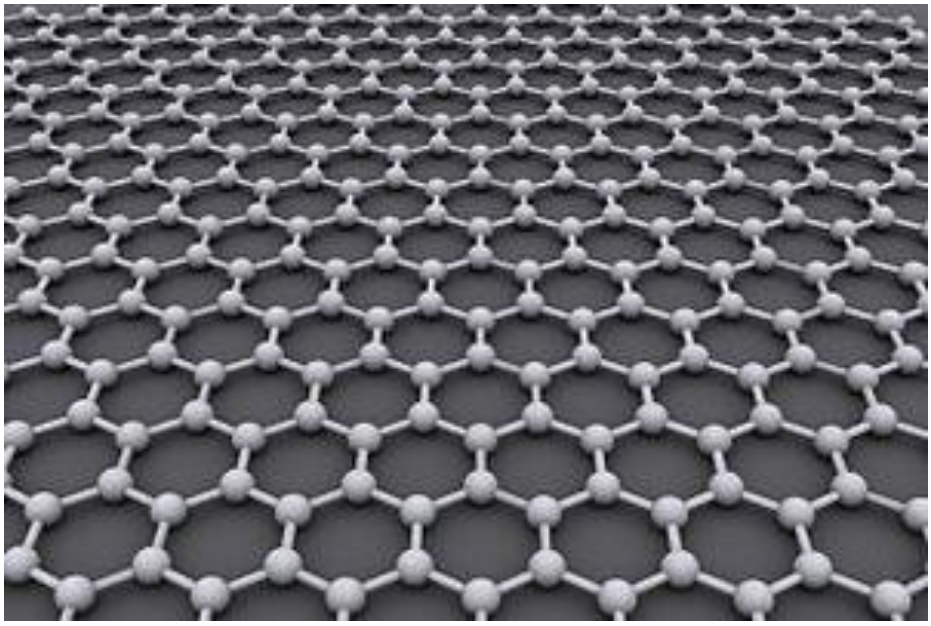

Figure 1.1 Graphene configuration

(http://en.wikipedia.org/wiki/Graphene)

1.2.3 Lignin

Lignin is one of the three major wood components and plays an important role in binding cellulose and hemi-cellulose together and providing support to the cell wall (Sjöström 1993). Lignin (Figure 1.2) has an aromatic structure and is composed mainly of p-coumaryl alcohol, coniferyl alcohol, and sinapyl alcohol through covalent linkages (Guo et al 2014). Lignin is the second most abundant renewable carbon source on Earth (Fisher and Fong 2014). Commercially, lignin is produced as a byproduct of the pulp industry. It can be utilized to produce graphene, activated carbon, carbon fiber, resin additive, and biofuel, etc.

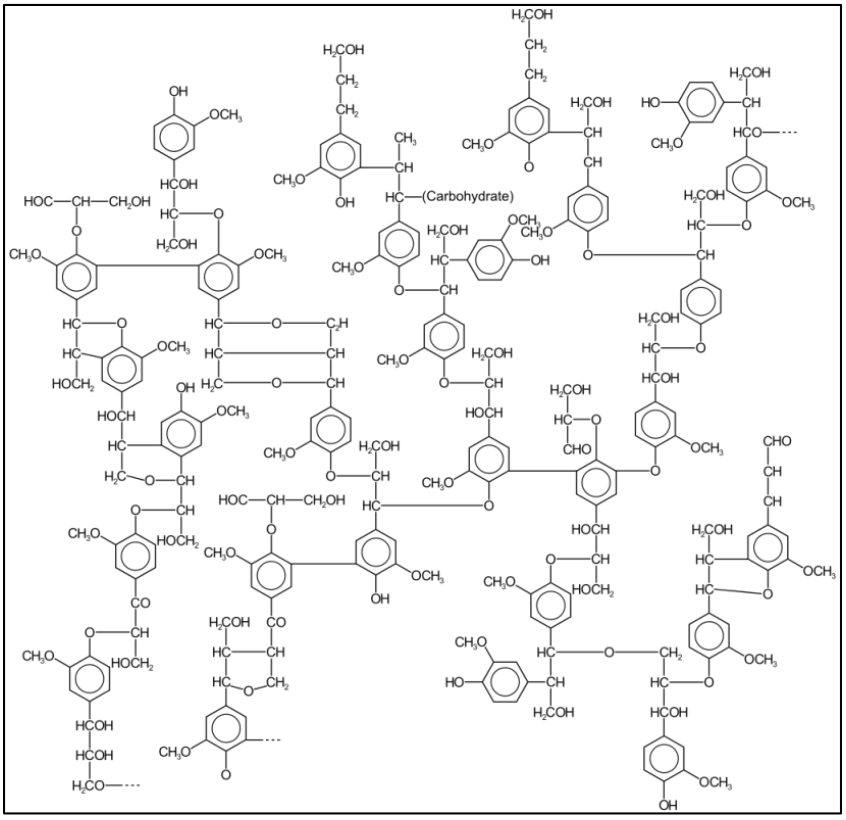

Figure 1.2 Lignin structure

(http://en.wikipedia.org/wiki/Lignin)

1.2.4 Known factors and mechanism on the growth of carbon encapsulated metal nanoparticles

Research on the carbon encapsulated metal nanoparticles has gained scientific interests recently. There are many superb properties of this material. Carbon encapsulated metal nanoparticles combine both the characteristics of metal and carbon together. They are highly conductive, thermally stable, have large electric capacity, functionalizable and can be used as a carrier for many other applications. Many transition metals can be selected for this purpose, including gold, silver, iron, nickel, copper, zinc, etc. (Laude et al 2007). A variety of methods can be utilized to synthesize the carbon encapsulated metal nanoparticles, including chemical vapor deposition (CVD), sputtering, carbon

implantation into catalyst substrate, etc. (Mwakikunga and Hillie 2011), of which CVD is a popular chemical method.

1.2.4.1 Chemical vapor deposition (CVD) method

The CVD method consists of a complex reaction system. The commonly agreed mechanism for the CVD method is schematically shown in Figure 1.3 (Zou et al 2013). Firstly, a carbon source is attached to the surface of the metal catalyst. The carbon source could be in the gas phase or solid phase.

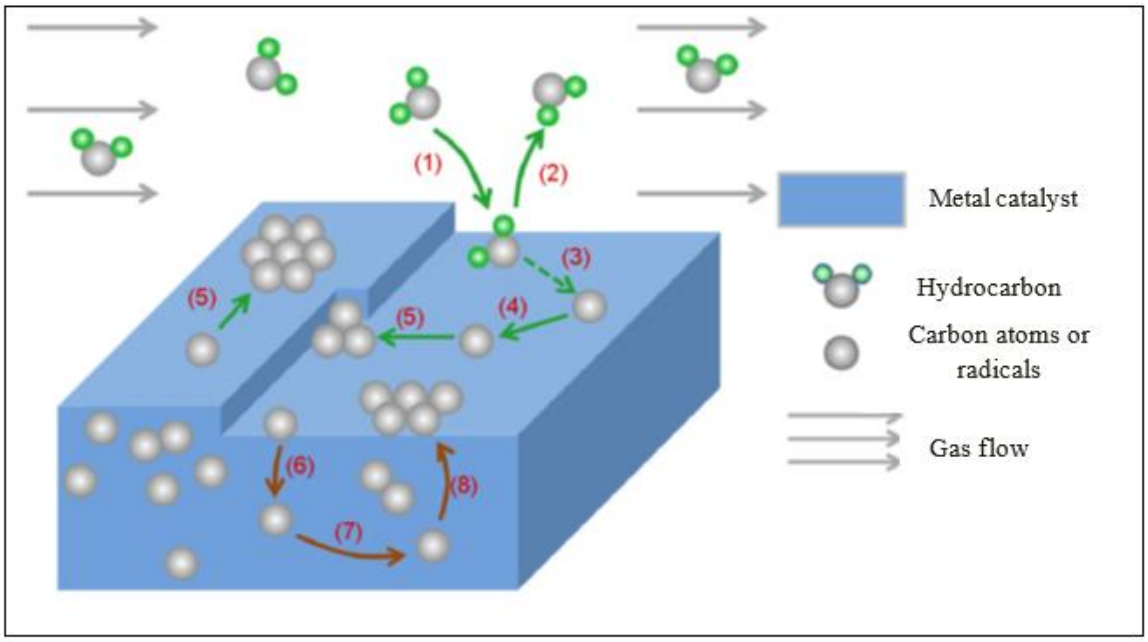

Figure 1.3 Reactions in CVD process

(Zou et al., 2013)

Part of the carbon source is detached from the surface by chance, while the other is decomposed into free carbon atoms as expressed by the following chemical equation.

$$2C_xH_y \xrightarrow{Metal\ catalyst} 2xC + yH_2 \quad (1.1)$$

The hydrogen gas will flow away from the surface (Ramón et al 2011).

There are two routes hereafter for the carbon atoms. One is called self-growth process, in which the graphene is formed directly at the defective sites such as corners, steps, etc. The other one is called dissolution-precipitation process. Metal has dissolving capacity for carbon atoms (Liu et al 2011), of which the saturation dissolution depends on temperature. The carbon atoms dissolve into the metal catalyst and diffuse within it by a carbon concentration gradient. The carbon atoms then precipitate onto the surface of the metal catalyst with the decrease of temperature, followed by the formation of graphene.

The graphene growth route is dependent on the types and nature of metal catalyst. For the metal catalysts that have a high capability to dissolve carbon atoms, the dissolution-precipitation route dominates the graphene growth. For those with poor dissolving capability, the self-growth route is the major route.

Carbon source, metal catalyst, temperature, temperature rising ramp, duration time, gas flow rate, and other parameters will affect the morphology, properties, and quality of the carbon encapsulated metal nanoparticles. The carbon source used by various researchers was selected according to the treatment method. In a typical CVD treatment, the carbon source usually originates from methane, acetylene, benzene, etc. (Ramón et al 2011, Laude et al 2007). In other treatment, 6H-SiC wafers (Li et al 2011) and carbon fibers (Jeong et al 2010) were also used as the carbon source.

Various transition metal catalysts were used, including Fe, Ni, Co, Cu, etc. These transition metals have different dissolving capacity for carbon atoms, which is determinant for the synthesis of graphene encapsulated metal nanoparticles. Fe, Ni, and Co have high dissolving capacity for carbon atoms. Carbon atoms could be easily dissolved into these metals and then precipitated onto the metal surface to form multi-layer graphene (Zou et al 2013). On the other hand, Cu has such a poor dissolving capacity for carbon atoms that the carbon atoms could only move onto the metal surface and form single or few-layer graphene. The metal catalysts studied existed in different forms, including metal nanoparticles (Li et al 2011), ions (Laude et al 2007), oxides (Mbuyisa et al 2012), and foil (Zhu et al 2010). In some studies, carbon source and metal catalyst existed in a single material, including metal organic compound, which would be decomposed when exposed under heat and leave the metal and carbon source in their original forms (Wang et al 2012).

Temperature plays an essential role in the growth of the carbon encapsulated metal nanoparticles. A wide temperature range was investigated by researchers (Laude et al 2007, Mbuyisa et al 2012, Li et al 2011, Gendy et al 2009, Jeong et al 2010, Song and Chen 2003, Sun et al 2012, Wang et al 2012). In some research, temperature of over 2000 ºC was used to heat the samples, and a satisfactory graphene structure was obtained. In most studies, mild temperature range (500-1000 ºC) was adopted. Amorphous graphitic carbon films mainly existed at around 580 ºC. When the temperature increased to 640-750 ºC, the carbon graphite was less amorphous, and continued to be more orderly with higher temperatures. Double heat treatment was another popular method used in the synthesis of carbon encapsulated metal nanoparticles. Firstly samples were heated at a

mild condition, followed by a higher temperature treatment. When compared to a single temperature treatment, better graphene structure of the product was believed to be obtained with double heating method.

Litter reaction was known under 500 ºC. Another area of research tacked an interesting question of how the carbon source and metal catalyst react before the growth of graphene. Instead of using the high temperature carbonization method, the non-thermal milling process was investigated (Motozuka et al 2012). It was found that Van der Waals attraction and/or binding force between the copper and carbon atoms resulted from the presence of oxygen atoms between them. The inter-lamellar binding force of the graphite aromatic ring was found to be weaker than the graphite sp^2 carbon-carbon bonding on the graphite aromatic ring.

Sample cooling rate was another important factor on the quality of the final products. In advanced experiment setup, there were two temperature zones, heat zone and cooling zone. The low temperature cooling zone could help the deposition of the graphene synthesized metal nanoparticles.

Shorter duration time was preferred to obtain products with better graphene structure. In the case of metal catalysts with high dissolving capacity for carbon atoms, shorter duration time suppresses the diffusion of remnant carbon atoms on top of the metal surface, thus generating smaller amount of amorphous carbon. In the case of metals with poor dissolving capacity of carbon atoms, increasing the duration time did not significantly improve the quality of the carbon encapsulated metal nanoparticles.

1.2.4.2 Thermodynamics and nucleation

In order to better understand the dynamics of the growth kinetics of graphene on the surface of metal nanoparticles, molecular dynamics simulation was studied (Meng et al 2012). The idea was to record desirable parameters for favorable graphene growth. A four-layer slab model of Ni (111) surface, which contains 256 Ni atoms in total or 64 per layer, was built to represent the catalyst surface. Three carbon concentrations (C_{16}, C_{32}, C_{64}) and four heating temperatures (527, 727, 927, 1127 ºC) were studied in the simulation. Results showed that at low carbon concentration (C_{16}), carbon atoms only diffused into the Ni matrix, without formation of large carbon sp^2 network, which was the requirement for the growth of graphene; as the concentration increased, graphene islands formed on the surface of Ni. Temperature played an important role in defect healing, which caused reconfiguration of 3-, and 4- member rings into more stable 5- and 6-member rings. 727 ºC was reported to be optimum for the growth of graphene, at which temperature maximum number of 6- member rings was obtained. When the temperature continued to increase to 927 and 1127 ºC, the inter-reaction between carbon and Ni was so active that some Ni atoms diffused out of the surface and made the substrate disordered.

The process of the nanoparticles growth is believed to encompass a stage called nucleation. The property of nucleus is considered very important, which would affect the following steps. The nucleus was assumed round in shape (Figure 1.4). The critical radius of nucleus for nucleation was dependent on many parameters, such as temperature, carbon-metal saturation coefficient, specific edge free energy, etc. (Kuznetsov et al 2001). The relationship was expressed in the following equation

$$r_{crit} = \frac{-(\epsilon + Q_c/4.5h)}{-(h/V_m)RTln(x/x_0)+(2\sigma_{graph}-W_{ad})} \quad (1.2)$$

Where ϵ was specific edge free energy, which can be estimated as the difference between the enthalpies of formation of C-C and metal-carbon bonds, divided by the distance between two neighboring carbon atoms, $r_{C\text{-}C}$; h was the height of nucleus; V_m was the molar volume of graphite; x/x_0 was the saturation coefficient; σ_{graph} was the specific surface energy of the basal plane of graphite; and W_{ad} was the work of adhesion of the graphite-metal system.

The nucleus was formed by several carbon atoms and grew further. The critical radius would increase with the decrease of temperature and saturation coefficient, and with the increase of the specific edge free energy.

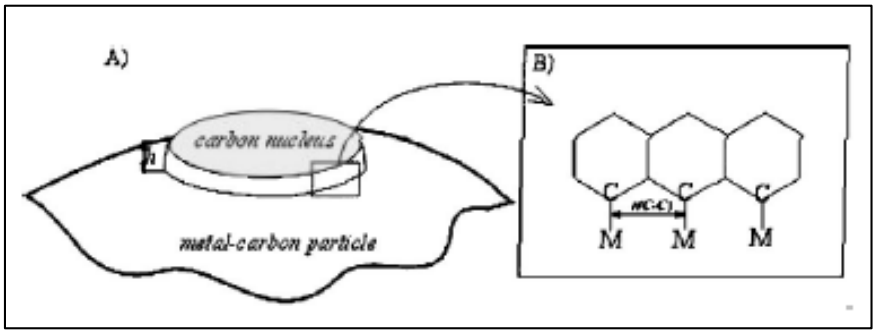

Figure 1.4 Schematics of carbon nucleus on the surface of the catalyst metal particle (Kuznetsov et al., 2001)

1.2.5 Functionalization

The goal of inventing the carbon shelled metal nanoparticles is to apply it in many areas, such as polymer nanocomposites, super-capacitor devices, drug delivery system, solar cells, memory devices, transistor devices, biosensors etc. (Kuila et al 2012).

Functionalization of the carbon shelled metal nanoparticles is indispensable to realize these applications.

Functionalization can be divided into two categories: covalent and non-covalent functionalization. Covalent functionalization involves surface re-hybridization of the C=C sp^2 configuration. Normally, covalent functionalization is achieved by nucleophilic substitution reaction, electrophilic substitution reaction, condensation reaction, and addition reaction (Kuila et al 2012). Non-covalent functionalization is achieved by creation of Vander Waals and electrostatic forces, applying stirring, sonication, heat application, etc.

A schematic diagram (Figure 1.5) shows different paths for covalent functionalization of graphene or graphite oxide. Route VI for example, depicts covalent grafting of RNH_2 groups onto the graphene oxide by acylation reaction between the -COOH group in the graphene oxide and alkylamine group from extraneous environment after activation of the –COOH groups with $SOCl_2$ (Loh et al 2010).

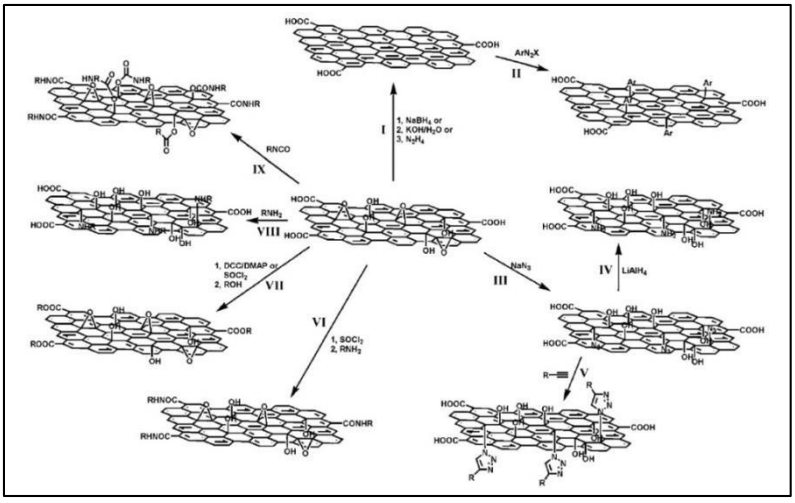

Figure 1.5 Covalent functionalization of graphene or graphite oxide (Loh et al. 2010)

One of the extensively studied functionalizing agents is dichlorocarbene. The cycloaddition of CCl_2 would change the graphene structure by pulling the carbon atoms out of the graphene plane (Zan 2014). The carbene group could possess electron accepting or donating features depending on the specific carbene group, which made it easy to react with graphene. Compared to the inner carbon atoms within the graphene plane, dichlorocarbene was much easier to graft on the edge carbon atoms, since the binding energy between them was higher than that between the dichlorocarbene and inner carbon atoms.

Acidification was another popular method of functionalization of carbon encapsulated metal nanoparticles. It was extensively investigated due to a commercial need of high loading of metal nanoparticles deposition on the carbon source. Acid could change the surface properties of the carbon nanoparticles, making it possible for further functionalization. Acid could react with carbon encapsulated metal nanoparticles and

introduce the -COOH group on the existing defect sites, without generating new defects, which could further react with the -NH_2 group (Taylor et al 2009). Specific functional groups could be attached onto the graphene surface, including epidermal growth factor (EGF), which is targeted to and ablates specific cancer cells.

1.3 Objectives

The main objectives of this research are to find a feasible method to synthesize carbon encapsulated metal nanoparticles using lignin as the carbon source, to develop a synthesis model, to control the quality, and to modify the carbon encapsulated metal nanoparticles with organic surfactant.

The detailed objectives are:

1) To validate the hypothesis that lignin and copper sulfate could be used to synthesize the carbon encapsulated metal nanoparticles.
2) To propose the synthesis model, either through gas deposition theory, or plastic film isolation theory.
3) To understand the evolution from lignin to graphene through a step-by-step study, and the role of metal in the evolution.
4) To study the effect of temperature, duration time, temperature rising ramp, and gas flow rate on the quality of the carbon encapsulated metal nanoparticles.
5) To modify the carbon encapsulated metal nanoparticles adding N-methyl-2-pyrrolidone, polyvinylpyrrolidone, and toluene, and to improve their dispersion properties in water, acetone, and ethanol.

The following chapters are written as a series of journal articles.

CHAPTER II

PRELIMINARY STUDY OF THE SYNTHESIS AND CHARACTERIZATION OF CARBON ENCAPSULATED COPPER NANOPARTICLES FROM LIGNIN

2.1 Introduction

Research on the carbon encapsulated metal nanoparticles (CEMNs) has gained scientific interests recently. There are many superb properties of this material: highly conductive, thermally stable (Gendy et al 2009), large electric capacity, functionalizable and can be used as a carrier for many applications. Many transition metals can be selected such as silver, iron, nickel, cobalt, etc. (Laude et al 2007). However, these magnetic metals are so active and have high dissolving capability of carbon that the synthesis process is difficult to control (Chae et al 2009). Compared to the magnetic metals, copper is a relatively less active transition metal, and has limited capability to dissolve carbon (Zou et al 2013). Thus the catalytic reaction can be easier to control.

Copper is the main component of regularly used wood preservatives, since it has toxicity toward microorganism in the free ionic state (Hingston et al 2001). However, insufficient fixation between copper and wood components results in the leaching problem. Carbon encapsulated copper nanoparticles (CECNs) have better compatibility with wood components, and form a stable complex. Less leaching would render lower requirement for retention rate.

Many forms of carbon source can be used to produce CECNs, from solid to gaseous phase. Compared to the popular gaseous carbon such as methane, lignin was selected as the carbon source in this study. Lignin is an important biomass, which is the main byproduct from kraft pulping. Lignin is in aromatic structure and mainly composed of p-coumaryl alcohol, coniferyl alcohol, and sinapyl alcohol through covalent linking (Guo et al 2014). Lignin is the second most abundant renewable carbon source on Earth. However, lignin has not been optimally utilized to produce high value products. It is mainly burned to generate energy onsite the factory. In this study, deionized water purified BioChoice lignin (BCL-DI), which is a kraft lignin, was used as the carbon source to synthesize the CECNs (Domtar Inc., Plymouth, NC).

Varieties of methods can be utilized to synthesize the CECNs, such as chemical vapor deposition (CVD), sputtering, carbon implantation into catalyst substrate, etc. (Mwakikunga and Hillie 2011), of which, CVD is a popular chemical path. Here a simple thermal treatment was applied to synthesize the CECNs using copper as the catalyst. Thermal treatment is a promising way for industrial scale up. Detailed synthesis process and characterization analysis were discussed in this paper.

2.2 Materials and methods

2.2.1 Materials

Deionized water purified BioChoice lignin (BCL-DI) was obtained from Domtar Inc. (Charlotte, North Carolina, USA). The basic information about the BCL-DI samples is shown in Table 2.1, and the element analysis data of the BCL-DI samples are shown in Table 2.2. Beetle-killed lodgepole pine (*Pinus contorta*) was supplied by USDA Forest

Products Lab (Madison, Wisconsin, USA). Copper (II) sulfate pentahydrate was purchased from Sigma Aldrich (St. Louis, Missouri, USA) and used as received.

Table 2.1 Basic information about lignin samples

Parameters\sample	BCL-DI
Weight(kg)	4.6
Moisture %	8.8
Ash%	0.2
pH	6.2
Lignin %	97.1
Sugar %	1.7
Solubility by water	Insoluble

Table 2.2 Element analysis results

Sample	N %	P %	K %	Ca %	Mg %	S %	Fe PPM	Mn PPM	Zn PPM	Cu PPM	Bo PPM
BCL-DI	0.16	0.02	0	0	0.01	0.03	40	17	6	3	20

2.2.2 Synthesis of Carbon Encapsulated Copper Nanoparticles (CECNs)

One part of $CuSO_4 \cdot 5H_2O$ and four parts of BCL-DI or Beetle-killed tree (oven-dry w/w basis, the weight of Cu was used to calculate the ratio between $CuSO_4 \cdot 5H_2O$ and BCL-DI) were dissolved into ten parts of distilled water. The mixture was heated at 80 ºC and kept stirring at hot plate stirrer for 12 h, followed by 24 h oven dry at 103 ºC. After that the mixture was ground in a mortar and pestle and stored in glass vial for later use.

Two porcelain boats, each holding around 1.5 g mixture, were place into a 50 mm diameter, 820 mm long quartz tube within the heating area. The end of tube was connected with an exhaust pipe and sealed with aluminum tape. Before heating, air in the system was excluded by flowing Argon gas for 15 min at a flow rate of 1800 sccm. Temperature was tuned up to 1000 ºC at a ramping rate of 10 ºC/min, and was held at 1000 ºC for 1 h, after which the sample was cooled down naturally until 200 ºC, and then

transferred to a desiccant for further cooling down. Argon gas was flowing during the whole process. The final weight of both samples was recorded and yield was calculated. Three replicates were selected in this experiment.

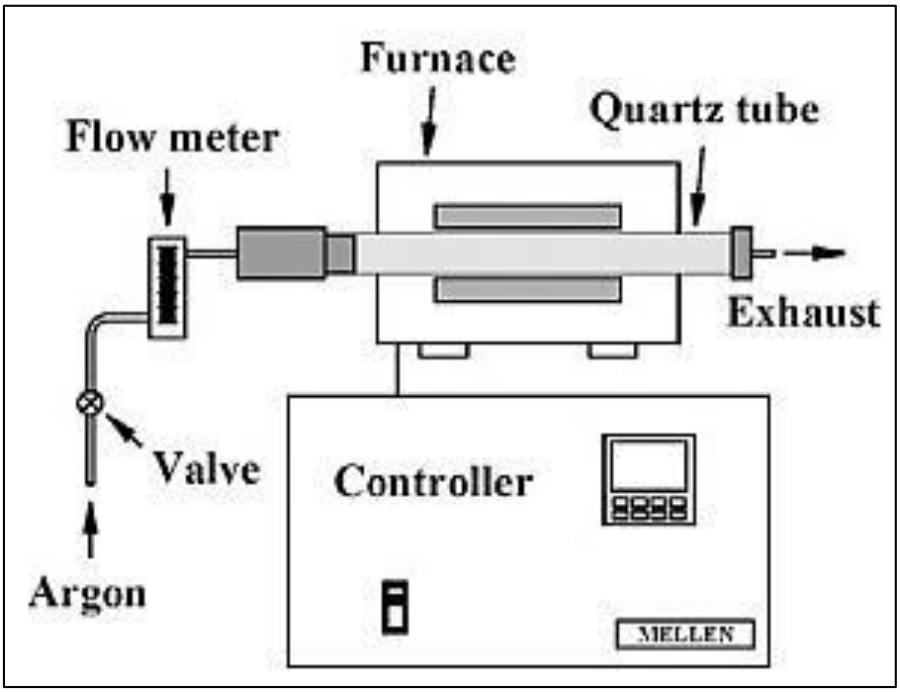

Figure 2.1 Scheme of thermal treatment

2.2.3 Characterization

2.2.3.1 XRD Characterization

CECNs powder was ground and analyzed with Rigaku SmartLab X-ray diffractometer (Rigaku, Woodlands, Texas) utilizing Cu Kα radiation (λ = 1.5418 Å). The scanning range was from 10-90 °, with a scan speed of 1 °/ min.

2.2.3.2 Microscopy

Sample for the SEM study was mounted on a carbon tape, and coated with platinum to improve its electric conductivity. It was completed on the JEOL JSM-6500F (JEOL, Peabody, Massachusetts). Sample for the TEM characterization was dissolved in acetone and sonicated for 15 min. One drop of suspension was dripped on a 300 mesh copper grid with lacey carbon film (Agar Scientific, Stansted, UK). The characterization was completed on the JOEL JEM-2100F (JEOL, Peabody, Massachusetts).

2.3 Results and discussion

2.3.1 XRD Spectroscopy

Since sample with Beetle-killed tree as the raw material did not successfully converted into CECNs, results will not be shown in this paper.

Four sharp peaks of different copper planes of atoms with much high intensity were shown in Figure 2.2, which masked the graphite peak at 2θ = 23-26 ° (Ju et al 2010). Low intensity of graphite peak indicated a poor yield of crystalline graphite. The reason was that less exposed area of copper was readily available for carbon atoms. When all exposed copper area was covered by carbon atoms, the graphite growth ceased, and surplus carbon atoms were blowed out as exaust gas or deposited on the graphite surface as the temperature went down and formed amorphous carbon. In future study, a design of higher ratio of copper to carbon should be tried and expose as much more copper area as possible, and then test whether the yield of crystalline graphite goes higher or not. The two peaks at 2θ =32.5 ° and 36.4 °, were characteristic for CuO (1 1 0) and Cu_2O (1 1 1), respectively. It meant that part of Cu atoms were oxidized to Cu^{1+} and

Cu^{2+} during the cooling process. These Cu was either uncovered or convered with defective graphite. These ionic copper could be easily washed out via HNO_3 purification.

Theoretically, the graphite peak should be at around $2\theta = 26.5$ °, the broad peak in Figure 2.2 indicated that both amorphous and crystalline carbon existed (crystal carbon means graphite in this paper). To some extent, there was more amorphous carbon than crystalline one. Gaussian function was applied to separate peaks and fit profiles. 4.8 % crystallinity was achieved in this experiment.

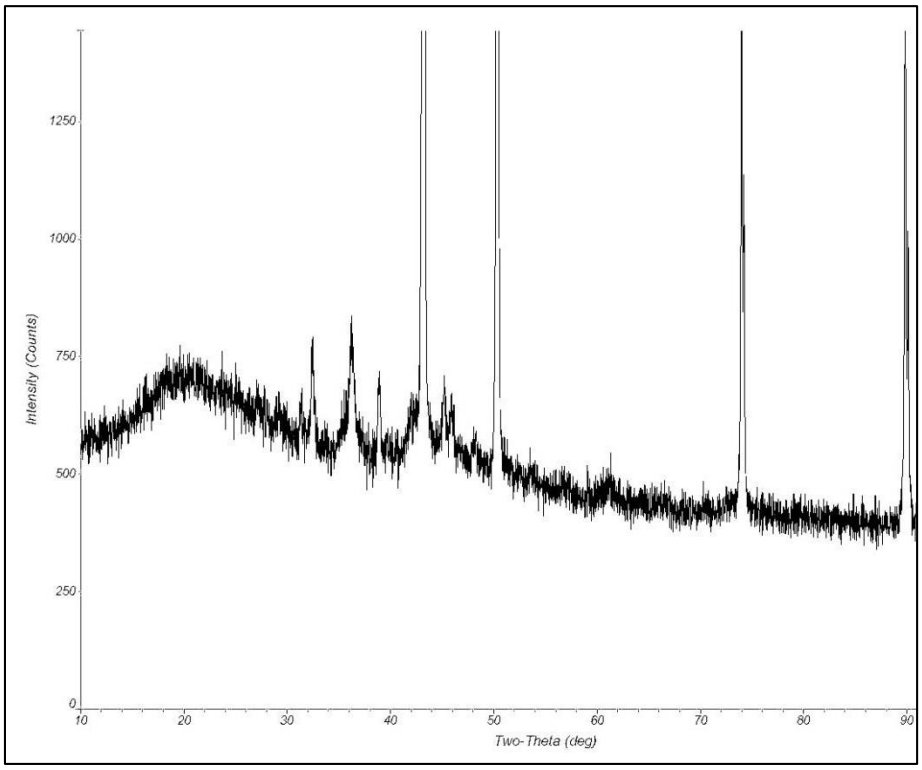

Figure 2.2 X-ray diffraction spectra of CECNs

2.3.2 Microscopy

Figure 2.3 shows scanning electron micrographs of CECNs. Layered structures were obvious at the cross section (refer to the arrow sign). As shown in Figure 2.3(a) and 2.3(b), CECNs were mainly located at the corners and steps, which were referred to as the defect area, indicating that the defect area was more favorable for copper to be localized and encapsulated with graphene. This finding was in agreement with the proposed mechanism by Zou and his coworkers (Zou et al 2013), which stated that copper had such a poor capability to dissolve carbon that carbon atoms mainly formed graphene layers at the defect sites. Figure 2.3(c) displayed folded graphite structure of CECNs at 30,000X magnification, which looked like a blossom flower. Defects mainly existed at the edge of the folded graphite. Further modification could be conducted at these sites.

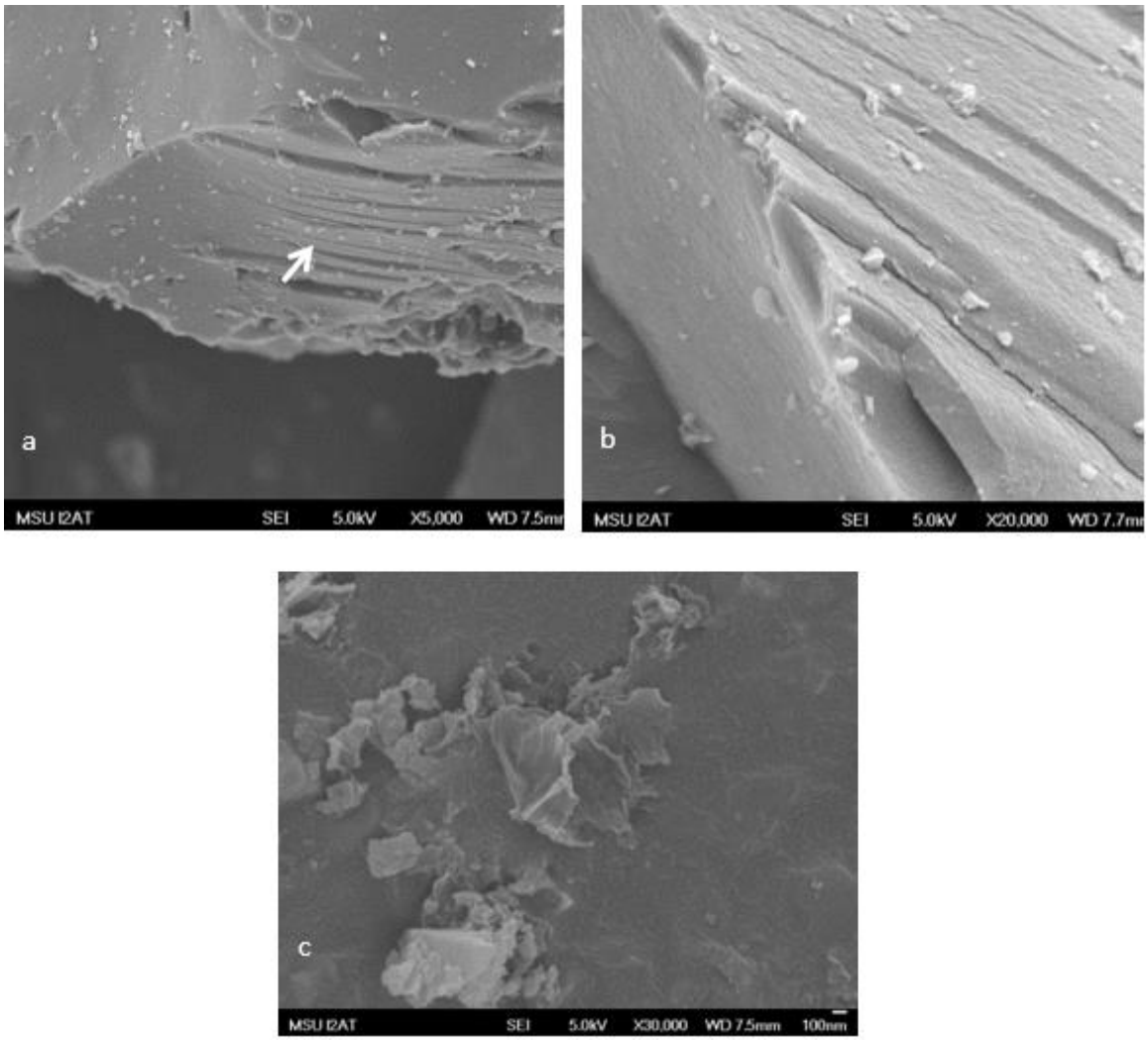

Figure 2.3 Scanning electron micrographs of CECNs at (a) 5,000 X. (b) 20,000 X. (c) 30,000X.

Figure 2.4(a) shows an overview of a large spot of CECNs. There were many copper nanoparticles encapsulated by graphite shells (refer to the arrow sign). The size of CECNs ranged from 10-30 nm, and the size distribution was uniform. Figure 2.4(b) was an enlarged photo of a single CECN. The 10 nm copper particle was encapsulated with only 2-3 layers of graphene. It was not normal to find graphite with dozens of layers. The reason was that CECNs were synthesized through the self-limiting mechanism: carbon

atoms barely dissolved into copper catalyst. Instead, they precipitated on the surface of copper and grew into single or few-layer graphene. As mentioned in the X-ray diffraction section, when all area of copper was covered with graphene, the growth progress ceased (Sun et al 2012). Figure 2.4(b) also revealed that the outmost layer of graphene shell was not perfectly sealed, there were defects. These defects could be used for many applications such as drug delivery and wood preservation. Drugs could be injected and stored inside the graphene through those defect sites, and then leached out and targeted to the bio-cell when it was transferred into the working area. However, functionalization of graphene needed to be done to make targeting and releasing drugs work. Similarly, CECNs could be grafted with functional groups, such as carboxyl, hydroxyl groups, and then tightly connected to wood cell wall. Copper would be released out slowly through the defective graphene shells and kill fungi and microorganisms. Leaching issue could be addressed by applying the modified CECNs as wood preservative, and lower retention rate could be required.

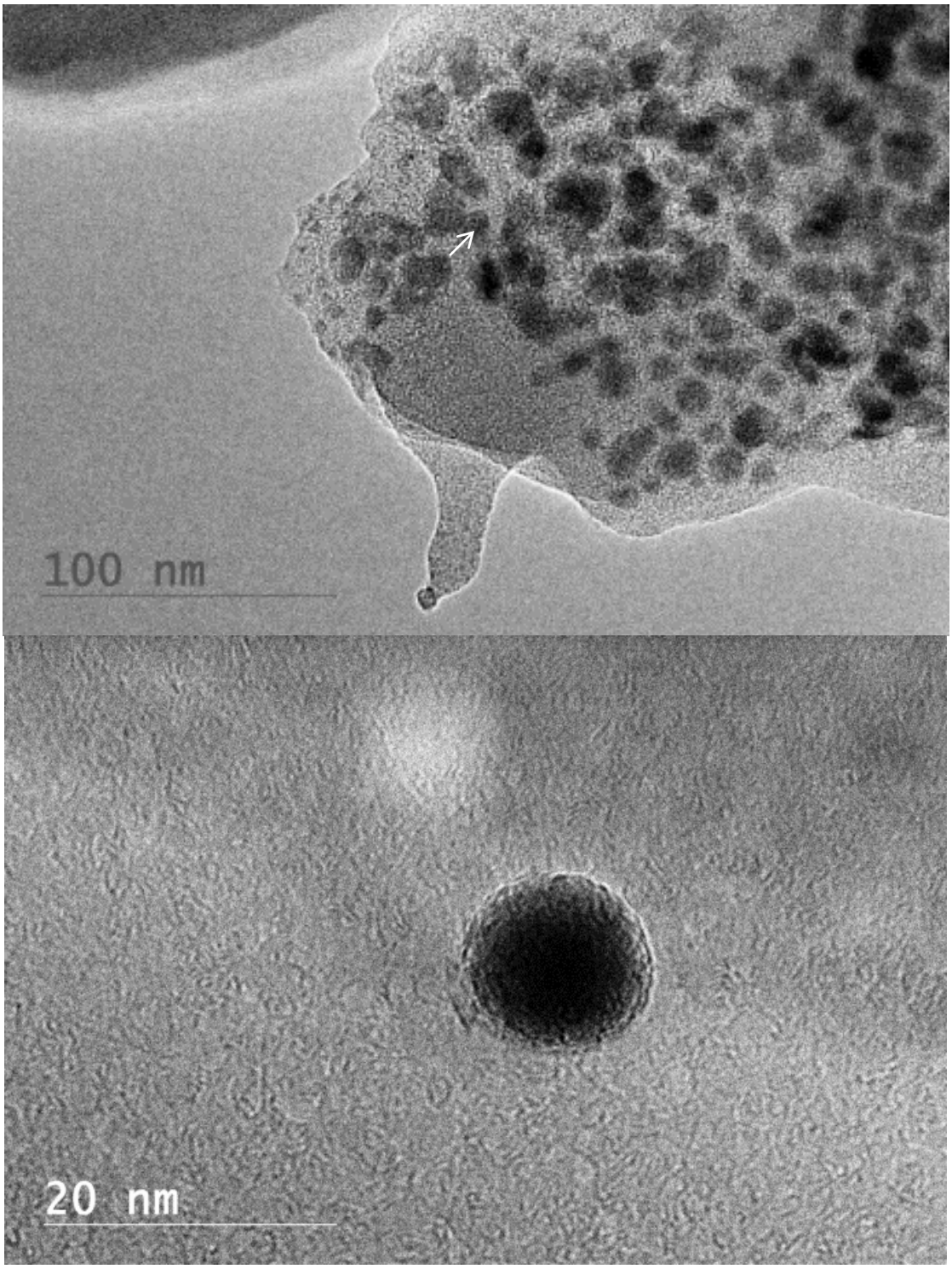

Figure 2.4 Transmission electron micrographs of CECNs

2.4 Conclusion

CECNs were successfully synthesized through thermal treatment at 1000 ºC. Samples were analyzed by X-ray diffraction, SEM, and TEM microscopy. The yield of graphene was limited. CECNs were mainly located at defect sites. Copper was found not tightly encapsulated by graphene shells. The size of CECNs was around 10-30 nm, with a uniform distribution. The defect structure of graphene might be utilized in bio medical application and wood preservation with further functionalization. Crystallinity of carbon material was low, amorphous carbon needs to be removed or converted into crystalline carbon. Future study should be focused on these areas.

2.5 References

Chae SJ, Günes, F, im KK, Kim ES, Han GH, Kim SM, Shin H-J, Yoon S-M, Choi J-Y, Park MH, Yang CW, Pribat D, Lee YH (2009) Synthesis of Large-Area Graphene Layers on Poly-Nickel Substrate by Chemical Vapor Deposition: Wrinkle Formation. Adv Mater 21(22): 2328-2333.

El-Gendy AA, Ibrahim EMM, Khavrus VO, Krupskaya Y, Hampel S, Leonhardt A, Büchner B, Klingeler R (2009) The synthesis of carbon coated Fe, Co and Ni nanoparticles and an examination of their magnetic properties. Carbon 47(12): 2821-2828.

Guo F, Shi W, Sun W, Li X, Wang F, Zhao J, Qu Y (2014) Differences in the adsorption of enzymes onto lignins from diverse types of lignocellulosic biomass and the underlying mechanism. Biotechnol Biofuels 7(1): 38.

Hingston J, Collins C, Murphy R, Lester J (2001) Leaching of chromated copper arsenate wood preservatives a review.pdf. Environ Pollut 111(1): 53--66.

Ju H-M, Choi S-H, Huh SH (2010) X-ray Diffraction Patterns of Thermally-reduced Graphenes. J Korean Phys Soc 57(61): 1649.

Laude T, Kuwahara H, Sato K (2007) FeCl2-CVD production of carbon fibres with graphene layers nearly perpendicular to axis. Chem Phys Lett 434(1-3): 78-81.

Mwakikunga BW, Hillie KT. (2011). Graphene synthesis, catalysis with transition metals and their interactions by laser photolysis. In Gong J (Ed.) Graphene synthesis, characterization, properties and applications. Intech.

Sun Z, Raji A-RO, Zhu Y, Xiang C, Yan Z, Kittrell C, Samuel E, Tour JM (2012) Large-Area Bernal-Stacked Bi-, Tri-, and Tetralayer Graphene. ACS nano 6(11): 9790--9796.

Zou Z, Dai B, Liu Z (2013) CVD process engineering for designed growth of graphene. Sci Sin Chim 43(1): 1.

CHAPTER III

STUDY OF THE FORMATION AND MECHANISM OF THE CARBON ENCAPSULATED COPPER NANOPARTICLES

3.1 Introduction

The carbon encapsulated metal nanoparticles were successfully synthesized by many methods, especially popular by chemical vapor deposition (CVD) growth (Li et al 2009). However, the graphene layers had defects. Efforts have been made to improve the quality of the graphene. Epitaxial growth of graphene under hydrogen gas environment showed an impressive improvement of graphene quality (Cai et al 2015). Hydrogen firstly helped build an active surface of carbon, which was crucial for the subsequent growth of graphene. Hydrogen also acted as an etching agent to eliminate defective sites and facilitate the growth of large scale graphene. However, the quality of the epitaxial graphene was influenced by the environment and quality of the deposition substrate. When under ethanol environment, the synthesized graphene had a poor quality, since an antigrowth reaction occurred and suppressed the deposition of graphene. While under ethylene environment in comparison, graphene with better quality was obtained (Maeda and Hibino 2013). Pretreatment of the substrate also played an important role in the growth of graphene, which could restore the defects of the substrate. SiH_4 pretreatment of SiC substrate resulted in the sublimation of Si after graphitization at

1250 °C, producing smooth surface of the substrate, hence, remarkably improved the quality of graphene (Sanbonsuge et al 2012). The air in the chamber was an obstacle for graphitization, which would react with the substrate and cause surface roughness. Silane flux pretreatment on a SiC surface could help dissolve the native oxide on SiC and passivate the surface of the substrate during graphitization, consequently improved the quality of graphene. In-situ SF_6 pretreatment also could help remove the native oxide by reacting with SiO_2 and generate SiF_4 gas. SF_6 pretreatment also had a benefit to increase the grain boundary and form large domain of graphene (Seo et al 2010).

Electrochemical pretreatment of metal catalyst could also effectively reduce the surface roughness of catalyst by etching the high protrusions. Hence, fewer nucleation sites were generated and large domain and high quality of graphene was obtained (Hsieh et al 2013).

Introducing a physical barrier was another effective way to improve the quality of graphene. The idea situation for the carbon atoms to grow into graphene was that carbon atoms started to grow right after the maximum process temperature was achieved. Introducing an Al_2O_3 barrier between carbon source and metal catalyst could retard the carbon diffusion process and reduce the pre-growth of graphene before reaching the maximum process temperature. The thickness of the Al_2O_3 barrier had a positive relation with the onset of growth temperature: the onset of growth was at a higher temperature when the thickness of the Al_2O_3 barrier was larger (Weatherup et al 2013). Since the premature growth of graphene was suppressed, the quality of the final graphene was improved.

The configuration of heating chamber and the placement of the metal catalyst could also affect the growth of graphene. The one-end-close configuration could restrict the carbon gas flow and consequently generate homogeneous graphene. The placement of metal catalyst would affect the concentration of the trapped carbon gas, subsequently could determine the number of graphene layers (Rümmeli et al 2013). The quality of graphene could also be improved by controlling the concentration of the carbon source and reducing the cooling rate during the CVD synthesis (Reina et al 2010). The concentration of carbon source was related to the number of graphene layers: maintaining a low concentration could result in the growth of mono- or bi-layer graphene. Reducing the cooling rate would largely decrease the nucleation sites of graphene, and make it possible to grow large domain of graphene. Moreover, a combination of direct current and CVD process could result in better graphene crystallinity and better surface morphology (Razak et al 2014). The direct current stress was believed to affect the grain growth of the metal catalyst, leading the growth of graphene to a better direction.

In this study, we investigated the CECNs forming process, and effects of mixture ratio of BCL-DI to copper catalyst on the improvement of CECNs quality.

3.2 Material and methods

3.2.1 Study of the CECNs forming process

Raw BCL-DI lignin with and without copper catalyst was investigated. The synthesis process can be referred to in Section 2.2.2. In this section, all BCL-DI samples with and without copper catalyst were heat treated from 200 ºC to 500 ºC, as shown in Table 3.1. XRD and FTIR-ATR spectra were obtained to analyze the CECNs forming process. XRD spectra was obtained from the Rigaku SmartLab X-ray diffractometer

(Rigaku, Woodlands, Texas) utilizing Cu Kα radiation (λ = 1.5418 Å). The scanning range was from 10-90 °, with a scan speed of 1 °/ min. FTIR-ATR spectra were obtained using Thermo Scientific™ Nicolet™ iS™50 FT-IR Spectrometer (Thermo Scientific, Waltham, Massachusetts). Samples were not purified with HNO_3, since the valence change of copper was to be analyzed.

3.2.2 Study of the effect of catalyst and ratio of copper sulfate pentahydrate to BCL-DI lignin on the crystallinity of CECNs

In this section, BCL-DI lignin and mixture of Copper Sulfate Pentahydrate and BCL-DI with four different ratios were used as the raw material (1:4, 1:2, 1:1, and 4:1, oven-dry w/w basis, the weight of Cu was used to calculate the ratio between Copper Sulfate Pentahydrate and BCL-DI). The synthesis process can be referred to in Section 2.2.2. Samples were heated at 600 ºC, 800 ºC, and 1000 ºC. The detailed process parameters are listed in Table 3.1. After the treatment, the sample with the ratio of 4:1 was stuck onto the porcelain boat and could not be transferred to the glass vial. The color of the final products was orange-red, typical for Cu atoms. The concentration of carbon was so low that all carbon source was oxidized into gas and only Cu atoms was left by the redox reaction. Samples with ratios of 1:4 and 1:1 were analyzed with XRD spectra.

Samples with copper catalyst were purified with 20 % HNO_3 before XRD and FTIR-ATR characterization. The purification process was elaborated as follows:

For each trial, 0.5 g CECNs was dissolved into 30 ml 20 % HNO_3 solution in a 125 ml conical flask. The suspension was then heated up to the boiling point and kept boiling and stirring for 30 min. The suspension was filtered by a membrane (pore size: 0.45 μm) (VWR, Radnor, PA) and rinsed with 550 mL deionized water. The residue was

dried in the oven at 60 °C for 6 h and then 103 °C overnight, weighed again, and stored in a glass vial for characterization.

3.3 Results and discussions

3.3.1 The carbonization yield

The carbonization yield was listed in Table 3.1. There were two assumptions for the calculation:

1). There was no reaction occurred during the mixing of lignin and copper sulfate;

2). Copper element kept the same weight during the carbonization process, while sulfur and oxygen were excluded in the gaseous form from the system.

$$\text{Yield} = ((m_{ma}-m_b)-(m_{mb}-m_b)*64/416)/((m_{mb}-m_b)*256/416)*100 \quad (3.1)$$

Where m_{ma} represents the mass of the boat and sample after the thermal treatment;

m_b represents the mass of the boat;

m_{mb} represents the mass of the boat and sample before the thermal treatment;

64/416 represents the fraction of copper in the mixture;

256/416 represents the fraction of carbon source in the mixture.

Sample with the mixture ratio of 4:1 that was heated at 1000 ºC, 30 min, 20 ºC/min ramp, and 1200 sccm gas flow rate created a negative yield under the calculation equation. The reason was that the fraction of BCL-DI lignin was much smaller than that of copper, and most of the lignin was gasified; moreover, during heating at 1000 ºC, part of the copper element was sublimated, while the calculation of yield did not consider the sublimated copper. The yield was underestimated.

In the situation at temperature lower than 250 ºC, the yield was equal to or more than 100%. It could be explained as that BCL-DI lignin has not started to decompose below 250 ºC, in the meantime, the copper ion was not reduced to copper atoms, and the SO_4^{2+} ion was not converted into SO_2 gas. Hence, the fraction of SO_4^{2+} was counted as BCL-DI lignin. In other words, the result was overestimated.

Table 3.1 Yield result for different treatment groups

Sample ID	Temperature ºC	Time min	Ramp ºC/min	Flow rate sccm	Ratio	Yield %
T1	1000	30	20	1200	4:1	-18.74
T2	1000	30	20	1200	1:1	33.76
T3	1000	30	20	1200	1:2	42.78
T4	200	30	20	1200	1:4	122.22
T5	200	30	20	1200	1:8	108.35
T6	250	30	20	1200	1:4	111.94
T7	250	30	20	1200	1:8	99.18
T8	300	30	20	1200	1:4	81.09
T9	300	30	20	1200	1:8	79.58
T10	400	30	20	1200	1:4	62.84
11	400	30	20	1200	1:8	60.63
T12	500	30	20	1200	1:4	53.91
T13	500	30	20	1200	1:8	54.38
T14	600	30	10	600	1:4	49.42
T15	800	30	15	1800	1:4	48.02
T16	1000	30	20	1200	1:4	46.57
T17	300	30	20	1200	-	54.04
T18	400	30	20	1200	-	41.09
T19	500	30	20	1200	-	38.30
T20	600	30	10	600	-	41.47
T21	800	30	15	1800	-	38.24
T22	1000	30	20	1200	-	37.30

Figure 3.1 shows the effect of temperature and ratio of copper to BCL-DI lignin on the carbonization yield. There was an abrupt decrease in yield from 300 ºC to 500 ºC for both mixtures and the raw BCL-DI lignin. The decomposition of lignin into CO, CO_2, and hydrocarbon gases mainly occurred at the temperature range from 300 ºC to 500 ºC, accompanied with great mass loss in this range. When temperature further went up to 1000 ºC, the yield did not change much, as shown in Figure 3.3, since the decomposition process almost finished at 300 ºC-500 ºC. The yield for mixtures with both ratios was similar at low temperature range, however, that for the raw BCL-DI lignin was much lower (Figure 3.1). The beginning of growth of graphene layers on the surface of the copper nanoparticles helped fix partial carbon source in the system; while for the raw BCL-DI lignin, graphene was not synthesized, and most of lignin was decomposed, hence lower yield was generated.

The effect of ratio of copper to BCL-DI lignin at 1000 ºC, 30 min, 20 ºC/min ramp, and 1200 sccm gas flow rate on the carbonization yield was also investigated (Figure 3.2). The overall trend of yield was decreasing with the reduced fraction of BCL-DI lignin. Reduced amount of BCL-DI lignin means large amount of copper ions. More carbon source was needed in order to reduce the copper ions into copper atoms, thus more gas was decomposed. Finally less carbon was yielded.

Compared to the yield of raw BCL-DI lignin, the addition of copper catalyst largely increased the carbonization yield. The role of copper catalyst was to fix graphene layers and amorphous carbon on the surface of the catalyst. At high temperature range (600 ºC- 1000 ºC), there was no big difference in yield, as shown in Figure 3.3. Once the

growth of the graphene layer was finished, adding more heat into the system did not impact the yield much.

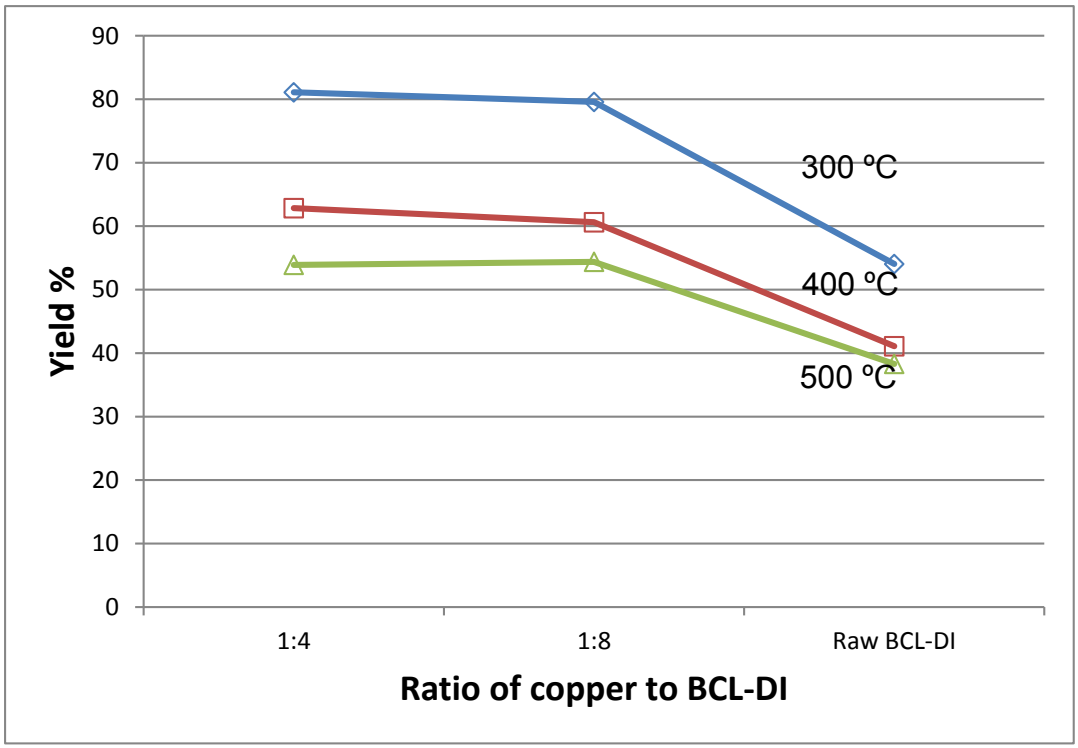

Figure 3.1 The effect of temperature and ratio of copper to BCL-DI on the carbonization yield

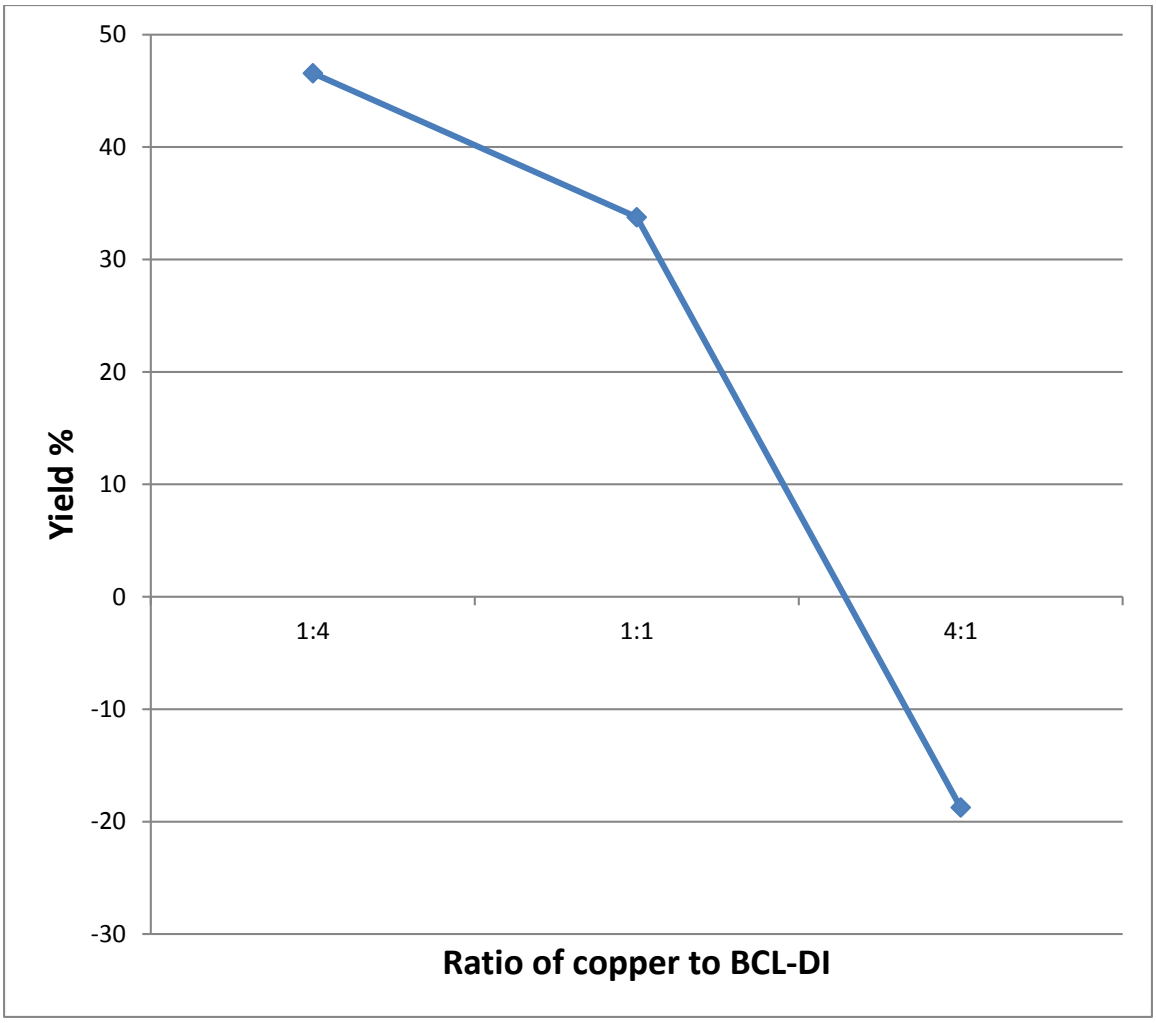

Figure 3.2 The effect of ratio of copper to BCL-DI on the carbonization yield at 1000 ºC, 30 min duration time, 20 ºC/min ramp, and 1200 sccm gas flow rate

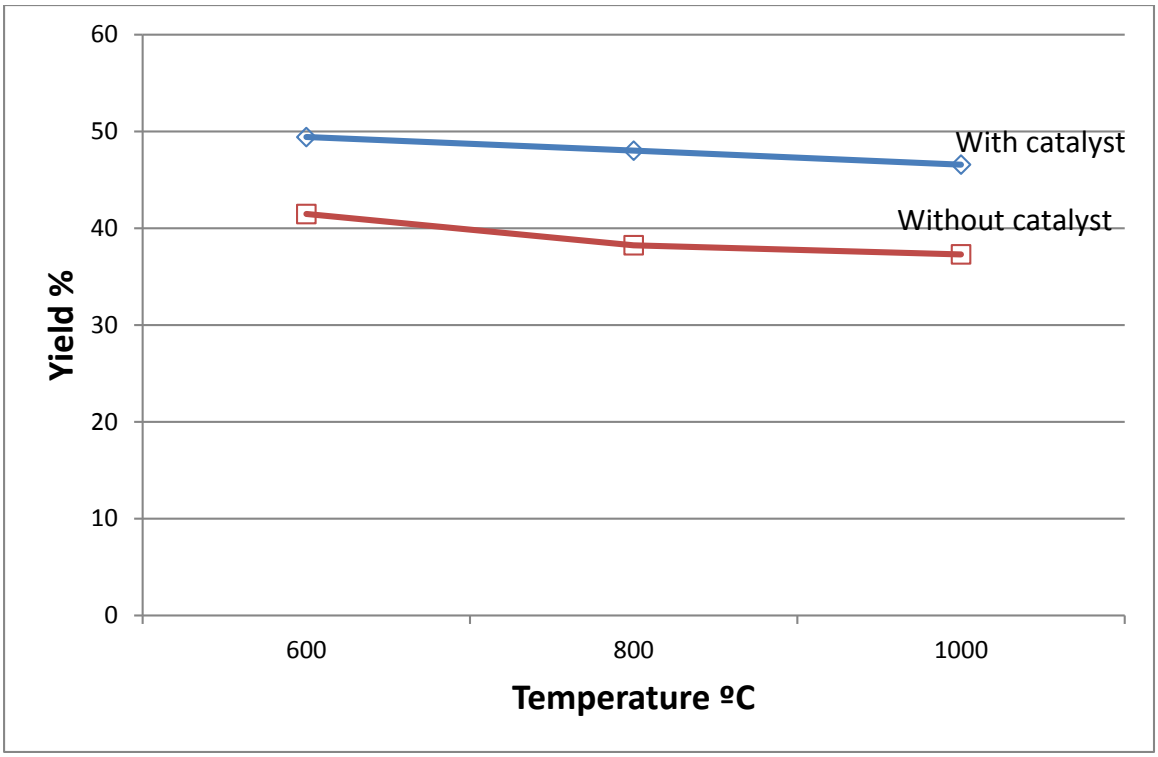

Figure 3.3 The effect of catalyst on the carbonization yield

3.3.2 The change of copper and BCL-DI lignin at low temperature range

XRD spectra of the mixture heated from 200 ºC to 500 ºC are shown in Figure 3.4. Copper element was existed mainly as Cu^{2+} and Cu^{1+} at 200 ºC and 250 ºC, only few were in the form of copper atoms, for sample mixed with both ratios. However, the situation changed when the mixtures were further heated up: for sample mixed with the ratio of 1:4, large amount of the copper ions were converted into Cu atoms at 300 ºC. All copper ions were converted into copper atoms from 400 ºC; while for that mixed with the ratio 1:8, copper ions were partially reduced and formed copper atoms at 200 ºC and 250 ºC. Then all peaks that were assigned to copper ions and atoms vanished as the temperature went up to 300 ºC and higher. The reason was unknown yet.

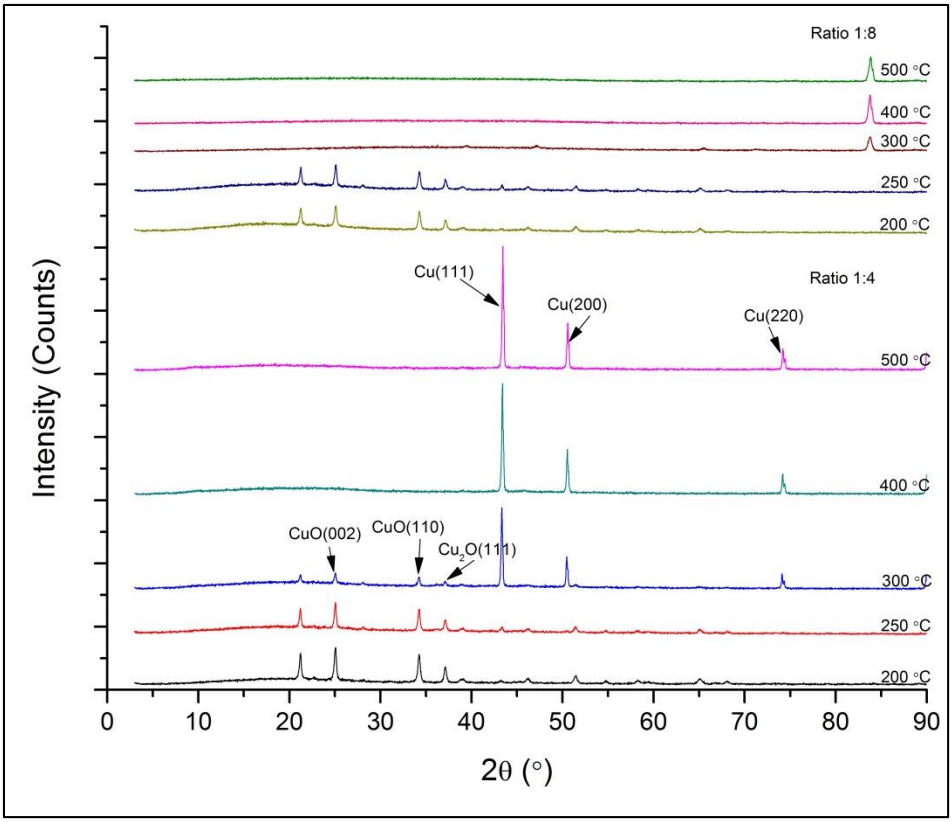

Figure 3.4 XRD spectra of mixture with a ratio of 1:4 and 1:8 treated from 200 ºC to 500 ºC

The oxidation reduction reaction occurred in accompany with the decomposition of BCL-DI lignin and formation of carbon gases, which is illustrated in the FTIR spectra in Figure 3.5. The intensity of the aromatic C=O bond at 1700 cm^{-1} went down with the increase of temperature. The breakdown of C=O bond resulted in the generation of CO, CO_2 gases (Yang et al 2007). The intensity of aromatic C=C bond at 1600 cm^{-1} did not reduce largely, since the bond was stable. However, with further increase of temperature, the other aromatic C=C bond at 1500 cm^{-1} vanished from 400 ºC. The C-H absorbance at 1450 cm^{-1} and wavenumber below 1000 cm^{-1} decreased as the temperature continuously went up. The C-O-C bond at around 1050 cm^{-1} vanished from 400 ºC. All these results

indicated that the phase of BCL-DI lignin changed abruptly above 300 ºC, which was coincident with the XRD data.

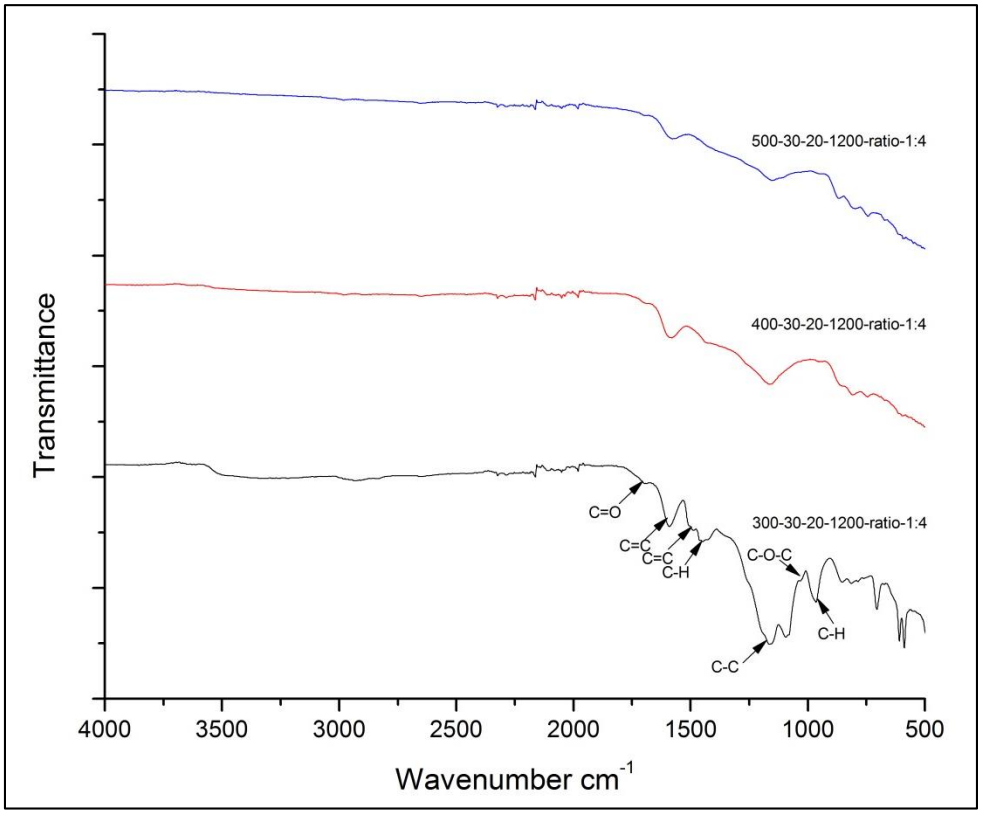

Figure 3.5 FTIR spectra of mixture treated at 300 ºC, 400 ºC, and 500 ºC, respectively (with a ratio of 1:4)

The changes of each functional group for sample with the mixed ratio of 1:8 were similar to that with the mixed ratio of 1:4, as shown in Figure 3.6.

We could conclude that the growth of amorphous carbon or graphene started at above 300 ºC, further details were shown via TEM images.

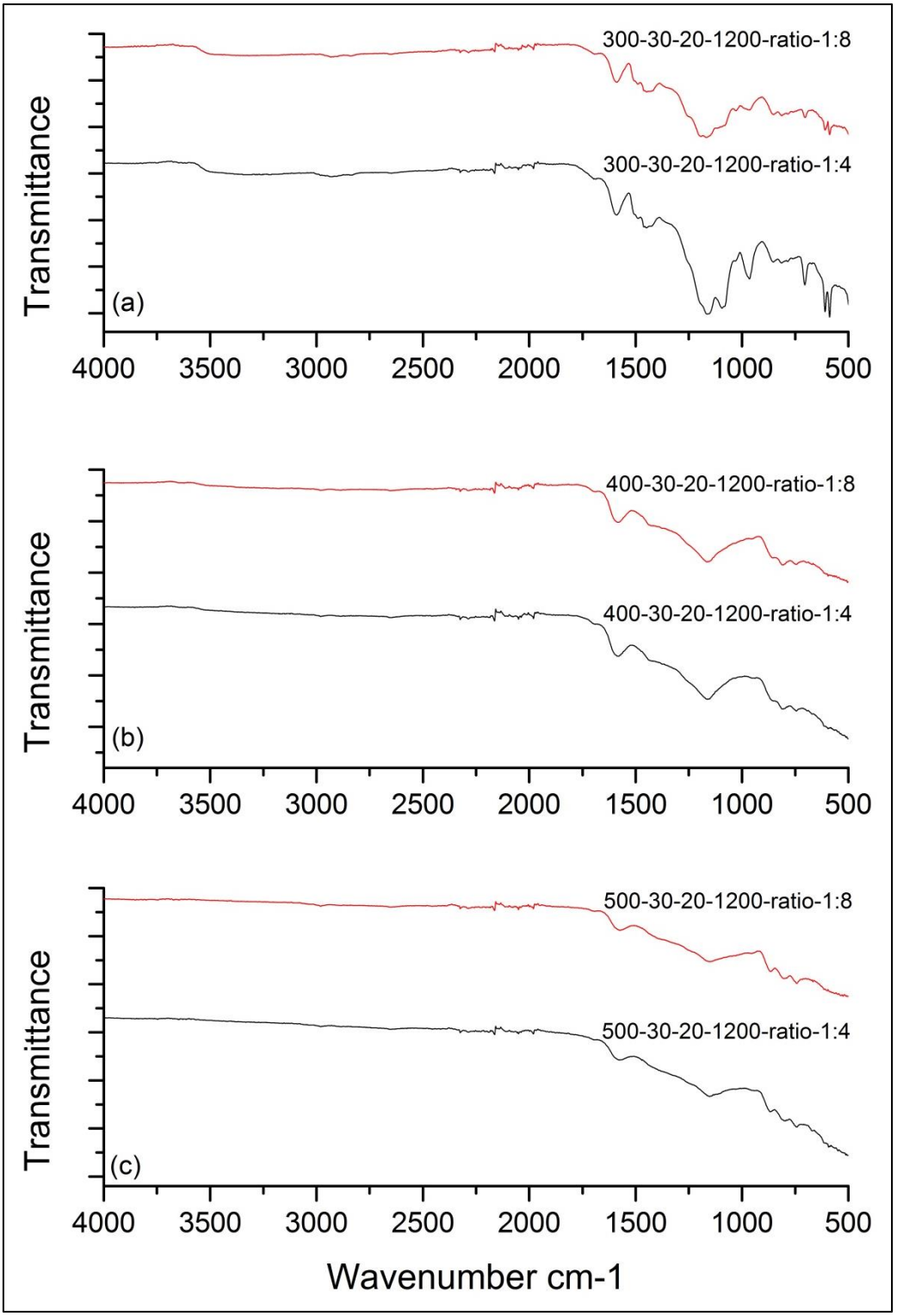

Figure 3.6 FTIR spectra of mixture treated at (a) 300 ºC, (b) 400 ºC, and (c) 500 ºC

The TEM images of samples that thermal treated at 300 ºC, 400 ºC, and 500 ºC are shown in Figure 3.7-3.9. The size distribution of nanoparticles was analyzed with the free ImageJ software (http://imagej.nih.gov/ij/index.html). Results are shown in Figure 3.7b, 3.8c, and 3.9c. The average diameter of nanoparticles was all less than 20 nm. The average size was decreasing with the increase of temperature.

There was no graphene layer covered on the surface of copper nanoparticles for samples heated at 300 ºC (Figure 3.7a). Amorphous carbon was probably existed; several graphene layers encapsulating the copper nanoparticles were located at the edge of the surface when the temperature went up to 400 ºC (Figure 3.8a). The number of layers was less than five. This finding confirmed that graphene layers were favorable to start to grow on the edges; further increasing the temperature to 500 ºC resulted in the synthesis of graphene shelled copper nanoparticles within the surface (Figure 3.9a). In addition, graphene bands at the connection sites between two domains were identified (inset of Figure 3.9a). These three graphs illustrated the evolution of graphene growth.

After HNO_3 purification, samples treated at 400 ºC and 500 ºC exhibit different evolution (Figure 3.8b, 3.9b). Almost all copper atoms were washed out after purification, as shown in Figure 3.8b. The inset image shows a defective graphene shell with two layers. Copper atoms could be easily in and out of this kind of shells. Sample treated at 500 ºC was more resistant to HNO_3, with many CECNs staying intact. The inset image in Figure 3.9b shows a less defective graphene shell with several layers of amorphous carbon covered on it. This finding confirmed that temperature played an important role in the growth of graphene. Graphene obtained at 400 ºC was proposed to

be a premature phase. Better quality of graphene should be synthesized at higher temperature.

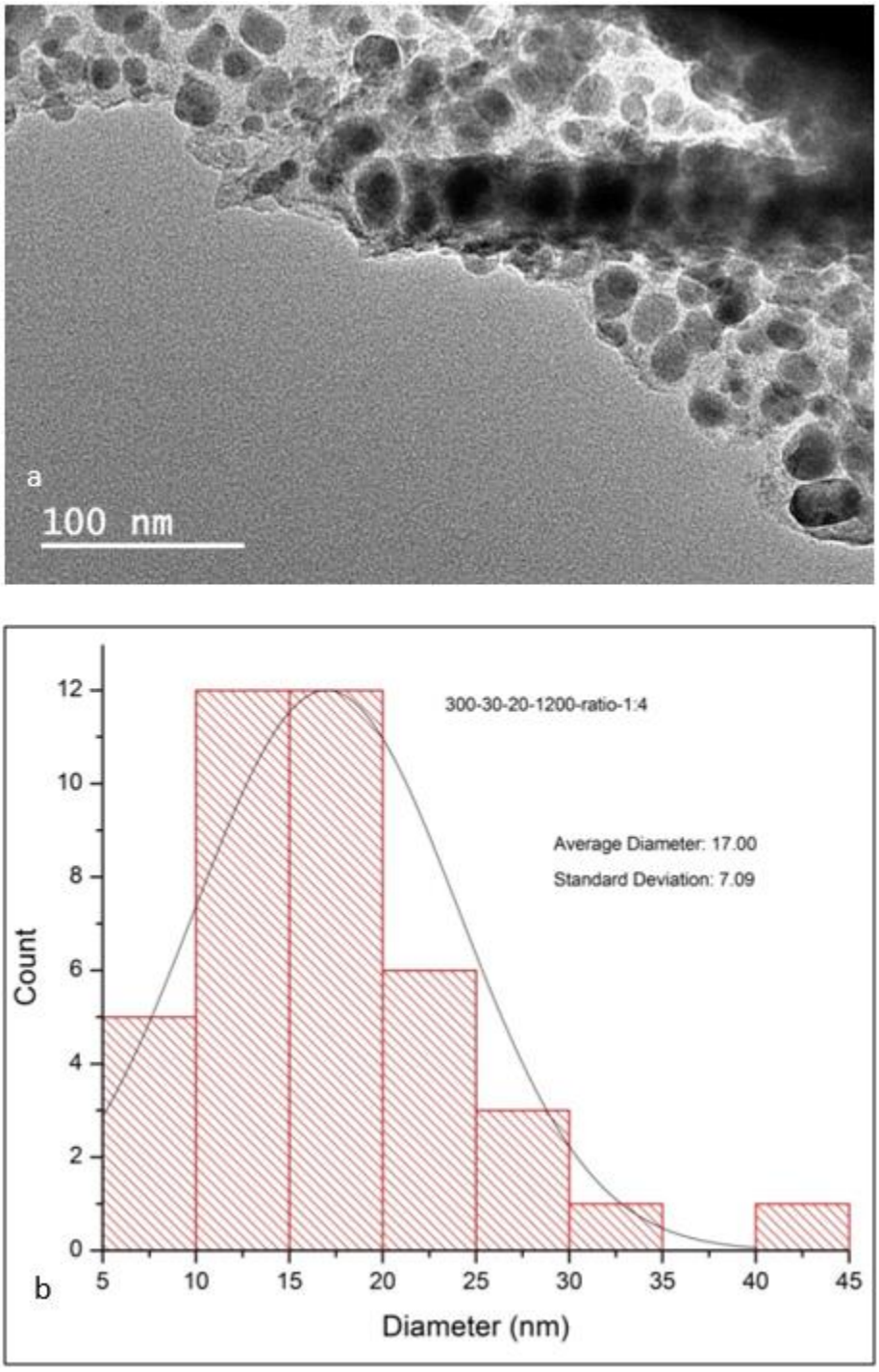

Figure 3.7 Sample treated at 500 ºC

(a) without HNO3 purification
(b) with HNO3 purification
(c) Particle size distribution

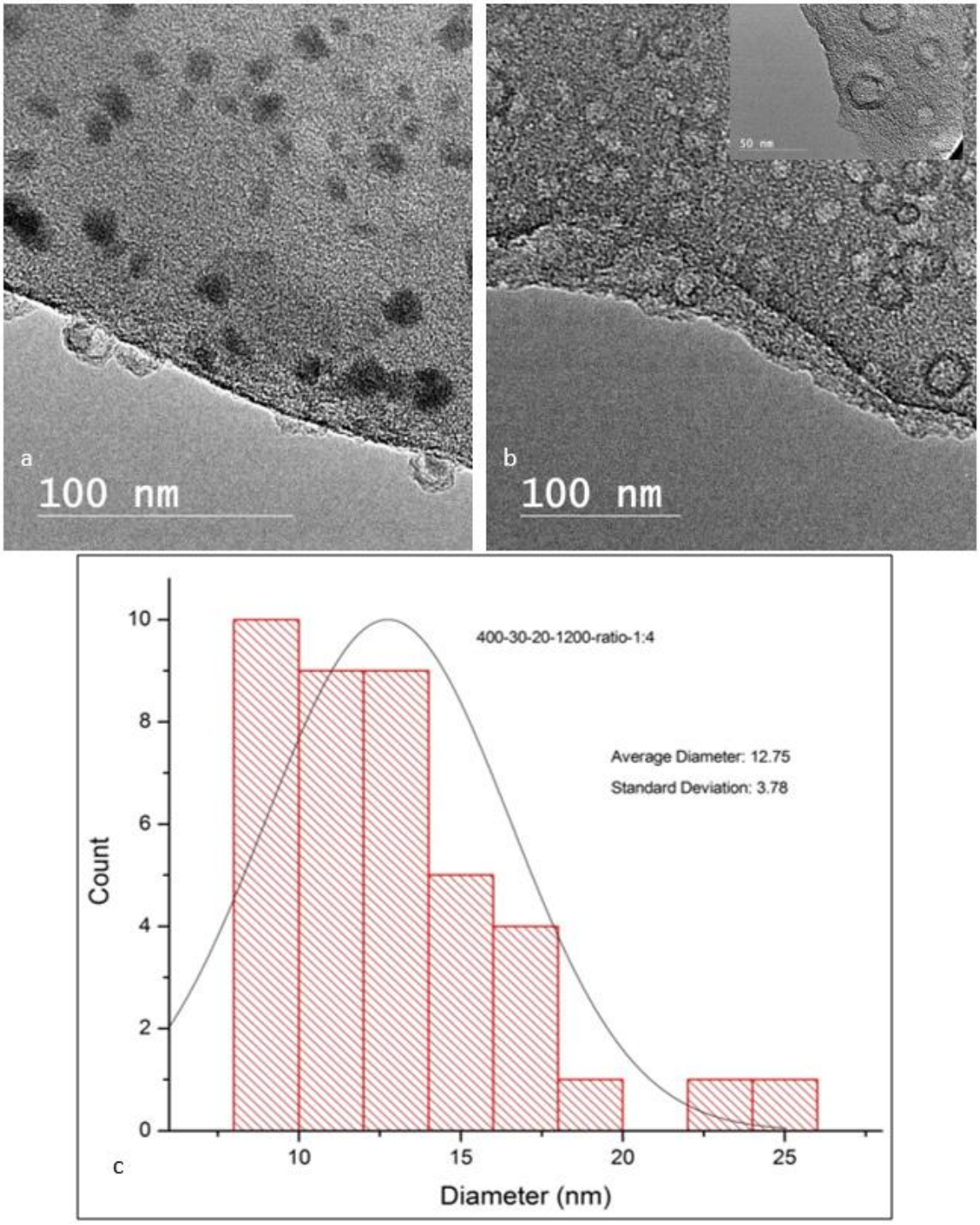

Figure 3.8 Sample treated at 400 ºC

(a) without HNO3 purification
(b) with HNO3 purification
(c) Particle size distribution

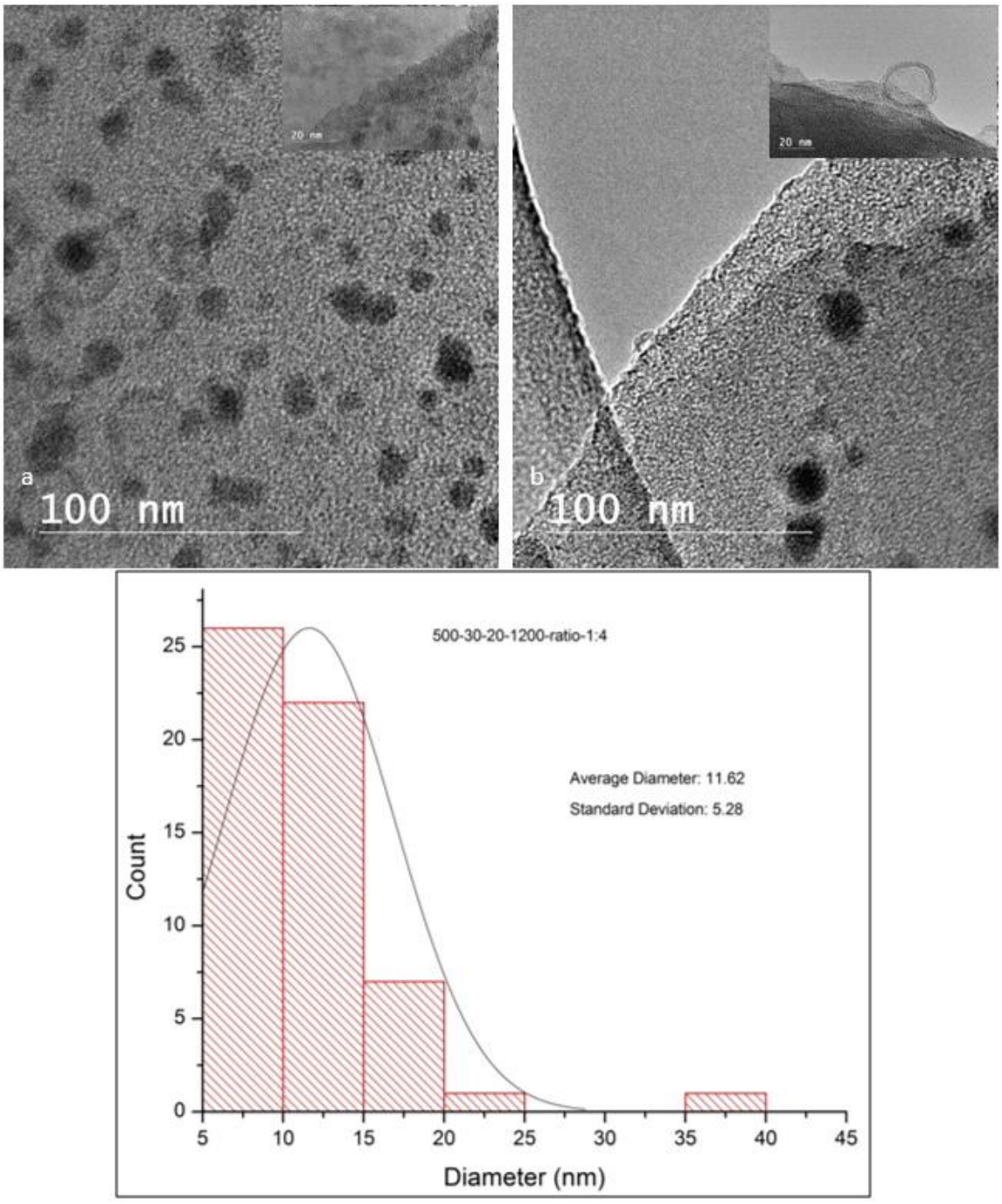

Figure 3.9 Sample treated at 500 ºC

(a) without HNO3 purification
(b) with HNO3 purification
(c) Particle size distribution

3.3.3 The effect of copper catalyst on the change of functional groups of BCL-DI lignin

The changes of functional groups of BCL-DI lignin were illustrated in Figure 3.10-3.12. When sample was heated at 600 ºC, 30 min, 10 ºC/min, 600 sccm gas flow rate without copper catalytic reaction, the spectra of functional groups was similar to that treated at 500 ºC. However, the one with copper catalyst showed weaker peak intensities. When sample was heated at 800 ºC, 30 min, 15 ºC/min, and 1800 sccm gas flow rate (Figure 3.11), and at 1000 ºC, 30 min, 20 ºC/min, and 1200 sccm gas flow rate without copper catalyst (Figure 3.12), there was no sign of function groups in the spectra. With the addition of copper catalyst, weak peaks could be located at around 1600 cm^{-1}, 1500 cm^{-1}, and lower than 1000 cm^{-1}.

It was proposed that from 600 ºC to 1000 ºC, copper was not only to decompose lignin, it also helped the growth of graphene layers, which was indicated by the increase of yield when copper was presented in the mixture. The disappearance of functional groups at 800 ºC and 1000 ºC also implied better quality of the final products, since almost only carbon atoms existed in the system, with no interruption by other atoms.

In previous section we proposed that the onset of growth of graphene layer was at 400 ºC, while here at 800 ºC and 1000 ºC, there must be a reconstruction of defective graphene layers, a reconfiguration of carbon atoms, and larger graphene domains were formed, thus higher quality of graphene was obtained.

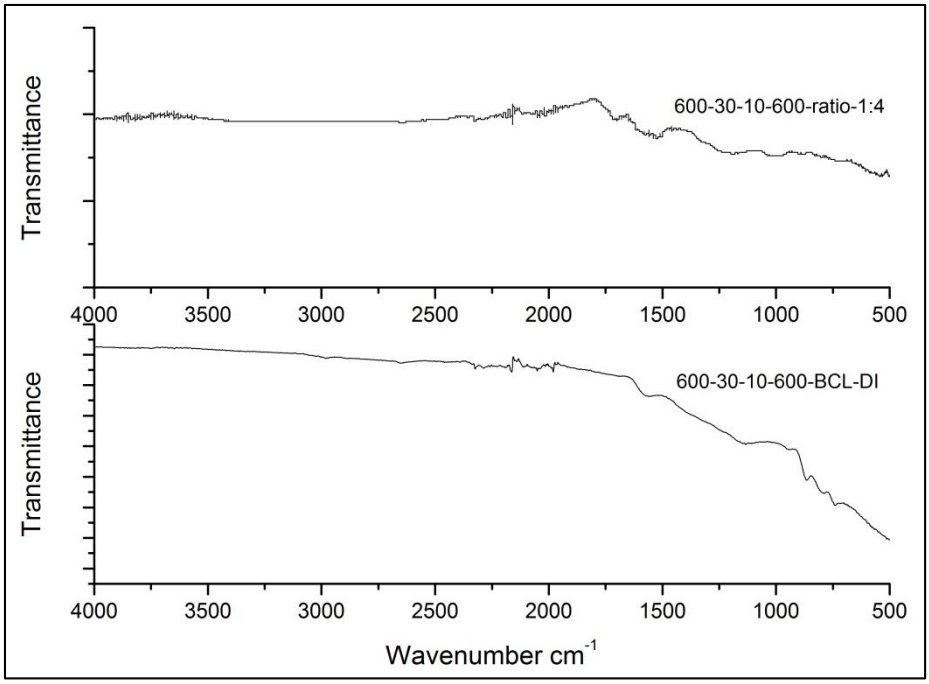

Figure 3.10 FTIR spectra of mixture treated at 600-30-10-600 with and without copper catalyst

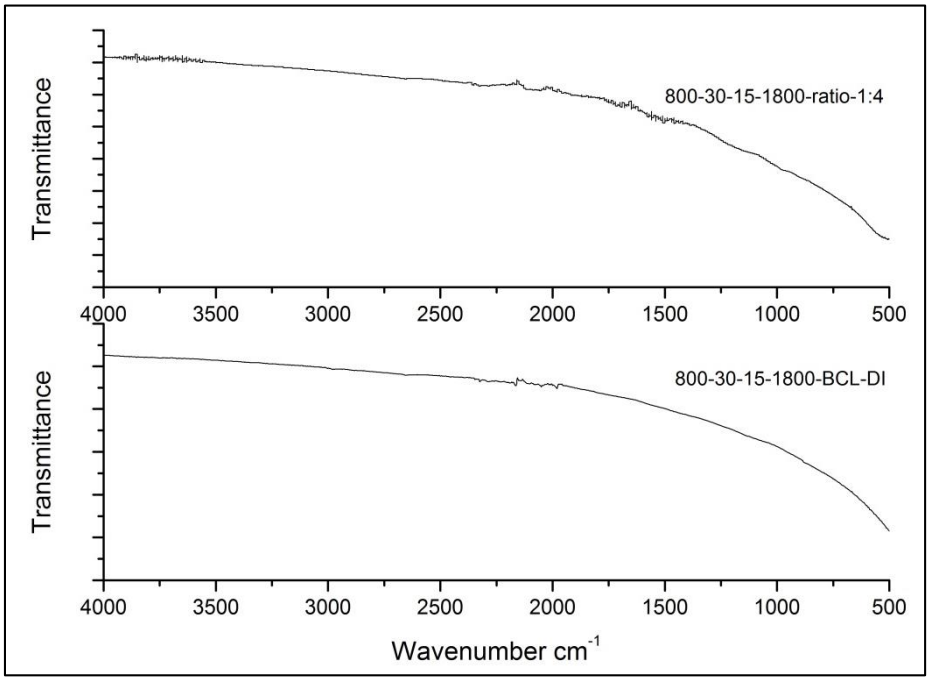

Figure 3.11 FTIR spectra of mixture treated at 800-30-15-1800 with and without copper catalyst

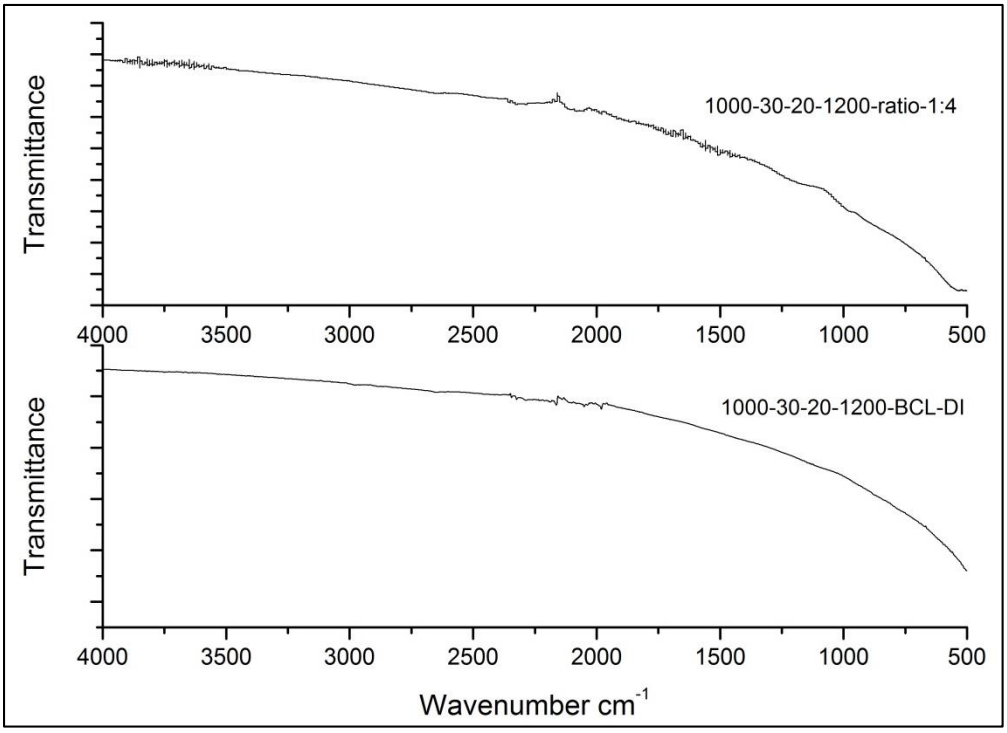

Figure 3.12 FTIR spectra of mixture treated at 1000-30-20-1200 with and without copper catalyst

3.3.4 The effect of mixture ratio and setup of sample placement on the crystallinity and morphology of CECNs

Figure 3.13 shows the XRD spectra of samples with two different mixture ratios: 1:4 and 1:1. The mixture with higher proportion of copper shows much higher intensity peaks at Cu (111), Cu (200), and Cu (220). In addition, the mixture also has a sharp Cu_2O peak that the one with lower copper proportion does not have, indicating that excessive copper atoms were oxidized during HNO_3 purification.

The crystallinity of graphite for the mixture with higher proportion of copper was higher than that with lower proportion of copper. Compared to the high intensity of copper peaks, the peak of graphite was still obvious. For the XRD spectra of previous

samples, when the peak of copper was high, that of graphite was barely shown in the spectra.

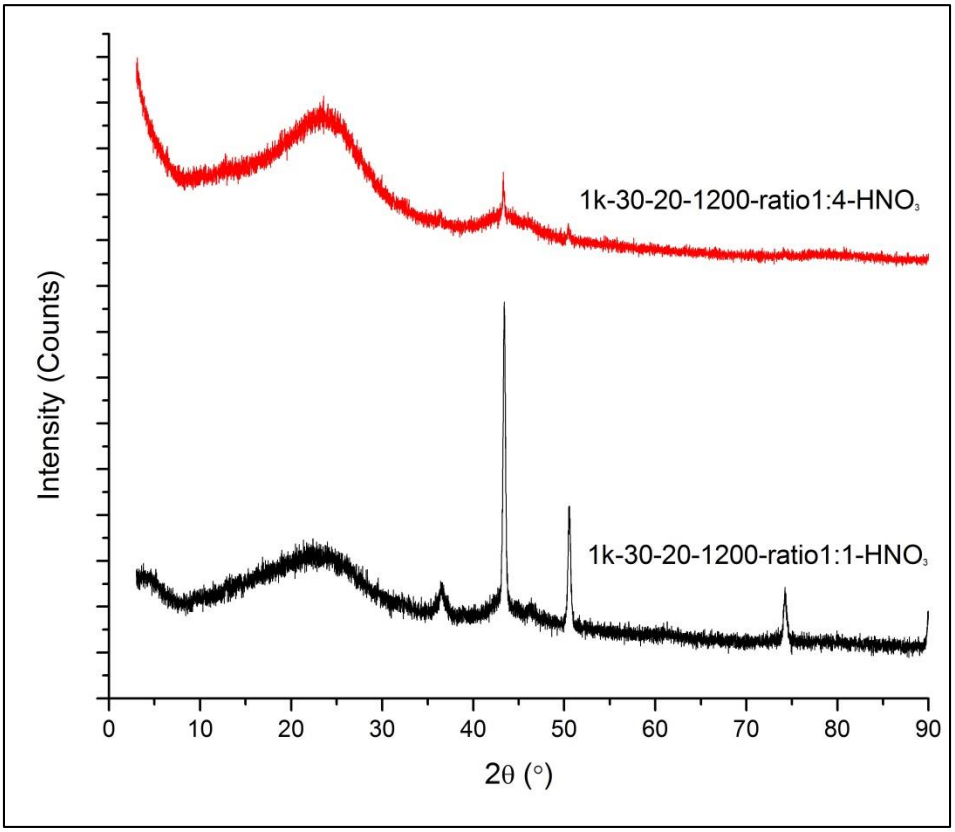

Figure 3.13 XRD spectra of mixture with a ratio of 1:4 and 1:1, respectively

The TEM graphs in Figure 3.14 illustrate uniformly distributed CECNs for samples with the ratio of 1:4, 1:2, and 1:1, which were treated at 1000 ºC, 30 min, 20 ºC/min, and 1200 sccm gas flow rate. The average diameter of CECNs was 8.41 nm, 11.81 nm, and 1.54 nm, respectively. Particle size decreased sharply for sample with the mixture ratio of 1:1. Graphene band was also observed clearly at the ratio of 1:1. Larger

amount of copper atoms catalytically facilitated the growth of graphene islands and subsequently formed large graphene domains.

In another setup of experiment, two porcelain boats were filled with different samples: the first boat was filled with BCL-DI lignin only, and the next one was filled with the mixture with a ratio of 1:1. In a parallel setup, the first boat was filled with the mixture with a ratio of 1:4, and the second one was filled with the mixture with the same ratio of 1:1. The purpose of this setup was to investigate the role of gas generated during the redox reaction in the synthesis of graphene under 1000 ºC, 30 min, 20 ºC/min, and 1200 sccm gas flow rate. The XRD spectra in Figure 3.15 shows no much change for each peak, implying that change in gas amount did not help the synthesis of graphene, or that the gases were flown out of the chamber with the argon gas before reaching the critical graphene synthesis temperature. In this experiment setup, the role of gaseous carbon was not important in the synthesis of CECNs. However, advanced experiment setup needs to be designed to trap the carbon gases before reaching the critical temperature, and then to investigate the role of carbon gases in the synthesis process.

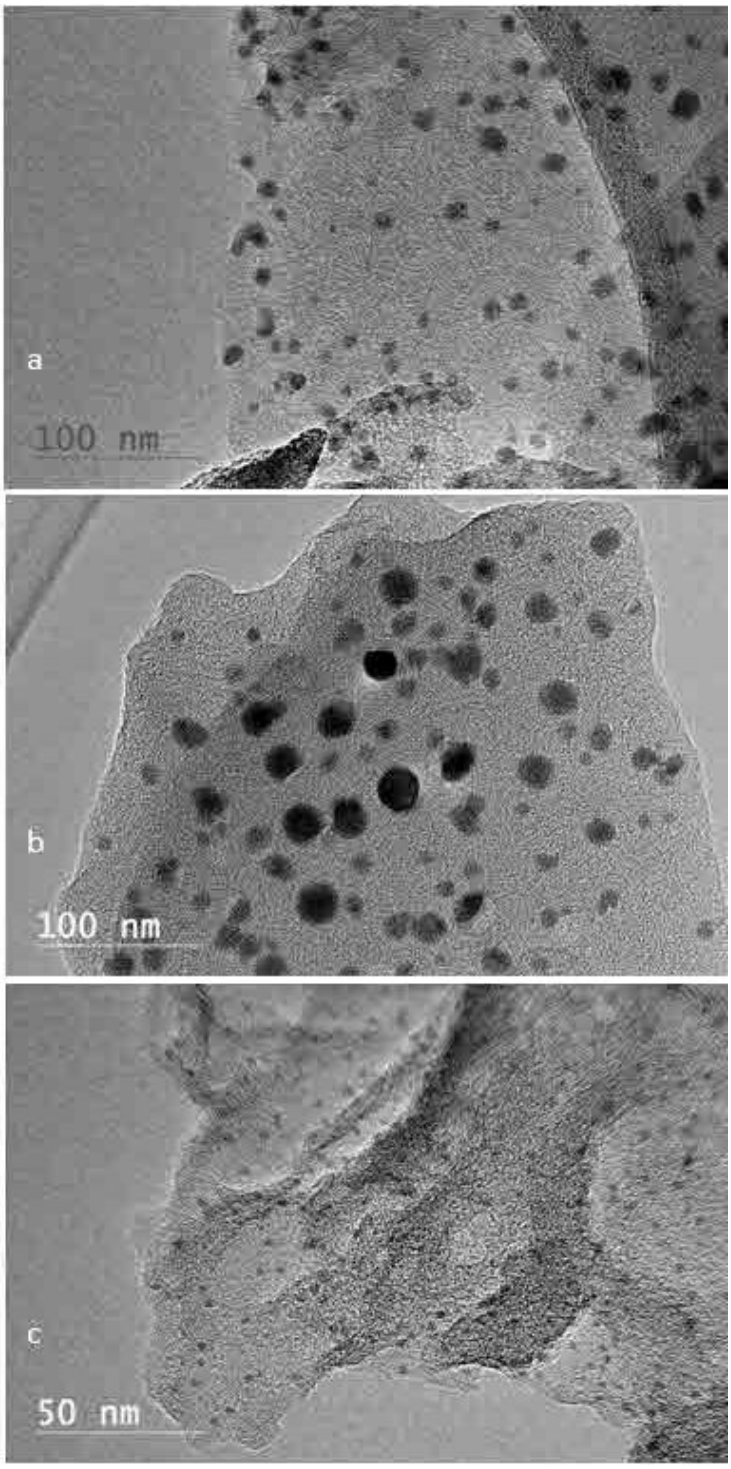

Figure 3.14 TEM images of mixture treated at 1000 ºC, 30 min, 20 ºC/min, and 1200 sccm gas flow rate

(a) mixture with the copper to BCL-DI lignin ratio of 1:4 (b) mixture with the copper to BCL-DI lignin ratio of 1:2 (c) mixture with the copper to BCL-DI lignin ratio of 1:1

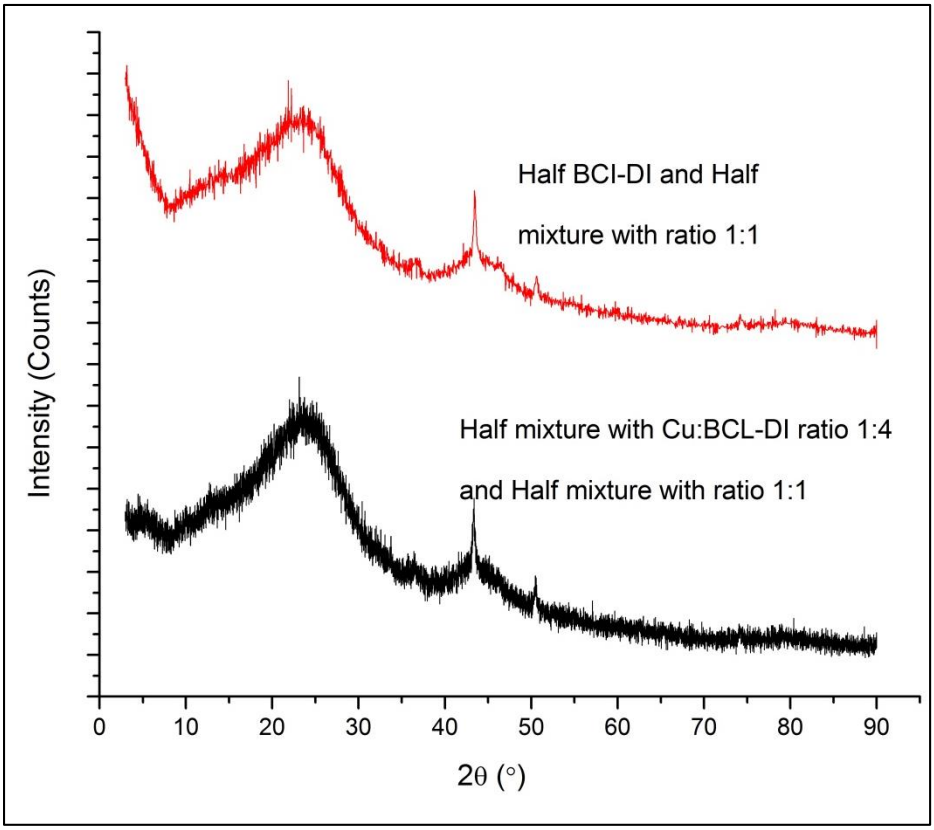

Figure 3.15 XRD spectra of two different sample setups

Red line: the first boat was filled with BCL-DI lignin, and the next one was filled with the mixture with a ratio of 1:1;
Black line: the first boat was filled with the mixture with a ratio of 1:4, while the second one was still filled with the mixture with a ratio of 1:1

3.3.5 The mechanism of the synthesis of CECNs

The graphene growth mechanism might be consisted of two phases. The first phase involved that lignin decomposed into short chain polymers and became soft, formed plastic film, and covered on the surface of copper nanoparticles, isolating it from contacting with other material. Lignin starts to melt at relatively low temperature (< 200 ºC) (Beis et al 2010). When heated at above 300 ºC, copper ions were converted into copper atoms. In the meantime, carbonaceous gases were formed through the redox

reaction. Since copper atoms have poor dissolving capacity of carbon, the plastic lignin film could only cover on the surface of copper nanoparticles and isolate them from any other contact. When heated to the critical temperature, the plastic lignin film started growing into graphene with the catalytic reaction by copper. Limited number of graphene layers could be synthesized since the isolation of copper catalyst from other forms of carbon. There were many defects on the graphene layers, because large amount of oxygen and hydrogen containing functional groups were still in the system. Excessive carbon would exist as amorphous carbon that covered on the graphene layers. However, when temperature was high enough, most of those functional groups were converted into volatile by-products, and only carbon atoms were left. Reconfiguration of carbon occurred, resulting in graphene layers with fewer defects. The amorphous carbon could even be converted into graphene without the help of copper catalyst (Lee et al 2013).

The second phase consisted of CO, CO_2, and hydrocarbon gases such as CH_4. CH_4 was widely used as the carbon source to synthesize graphene, and it was generated at a wide range of temperature (Yang et al 2007). CH_4 would be deposited on the available surface of copper nanoparticles and grow into graphene.

Both phases contributed to the synthesis of CECNs. The gas phase theory might contribute little in this study, as being proved in Section 3.3.4. Our previous attempt to synthesize CECNs using beetle-killed tree as the raw carbon source turned out to be a failure. The beetle-killed tree can also produce gas under thermal treatment, however, no sign of CECNs was observed, which at least on the other side proved that gas theory was not dominant in our study. The different placement setup in Section 3.3.4 also confirmed that there was no big difference in the crystallinity of CECNs by variation of the amount

of carbonaceous gas. The plastic film theory was dominant in this experiment, which could successfully explain the synthesis of few-layer CECNs.

3.4 Conclusion

The graphene forming process and changes of copper valence were investigated from 200 ºC to 500 ºC. Abrupt conversion of copper ions into copper atoms occurred at above 300 ºC, with the company of decomposition of BCL-DI lignin into CO, CO_2, and hydrocarbon gases. The growth of graphene layers was proposed to start at above 300 ºC. TEM images illustrated the onset of growth of graphene at the edge of the surface at 400 ºC, and the formation of graphene bands at 500 ºC.

The effect of copper catalyst on the synthesis of CECNs was studied from 600 ºC to 1000 ºC. Copper catalyst facilitated the decomposition of lignin functional groups at 600 ºC. Further increasing the temperature retarded the degradation of lignin, while assisted the reconfiguration of the defective sites of the graphene layers, producing higher quality products.

It was proposed that plastic film of BCL-DI lignin dominated the synthesis of CECNs, while gaseous phase of carbon had little impact.

3.5 References

Beis S, Mukkamala S, Hill N, Joseph J, Baker C, Jensen B, Stemmler E, Wheeler C, Frederick B, Heiningen VA, Berg A, DeSisto W (2010) Fast pyrolysis of lignins. Bioresour 5(3): 1408--1424.

Cai T, Jia Z, Yan B, Yu D, Wu X (2015) Hydrogen assisted growth of high quality epitaxial graphene on the C-face of 4H-SiC. Appl Phys Lett 106(1): 013106.

Hsieh Y-P, Wang Y-W, Ting C-C, Wang H-C, Chen K-Y, Yang C-C (2013) Effect of Catalyst Morphology on the Quality of CVD Grown Graphene. J Nanomater 2013: 1-6.

Lee S, Hong J, Koo JH, Lee H, Lee S, Choi T, Jung H, Koo B, Park J, Kim H, Kim Y-W, Lee T (2013) Synthesis of Few-Layered Graphene Nanoballs with Copper Cores Using Solid Carbon Source. ACS Appl Mater Interf 5(7): 2432-2437.

Li X, Cai W, An J, Kim S, Nah J, Yang D, Piner R, Velamakanni A, Jung I, Tutuc E, Banerjee SK, Colombo L, Ruoff RS (2009) Large-area synthesis of high-quality and uniform graphene films on copper foils. Sci 324(5932): 1312-1314.

Maeda F, Hibino H (2013) Molecular beam epitaxial growth of graphene using cracked ethylene. J Cryst Growth 378: 404-409.

Razak LA, Tobino D, Ueno K (2014) Improvement of multilayer graphene quality by current stress during thermal CVD. Microelectron Eng 120: 200-204.

Reina A, Thiele S, Jia X, Bhaviripudi S, Dresselhaus MS, Schaefer JA, Kong J (2010) Growth of large-area single- and Bi-layer graphene by controlled carbon precipitation on polycrystalline Ni surfaces. Nano Res 2(6): 509-516.

Rümmeli MH, Gorantla S, Bachmatiuk A, Phieler J, Geißler N, Ibrahim I, Pang J, Eckert J (2013) On the Role of Vapor Trapping for Chemical Vapor Deposition (CVD) Grown Graphene over Copper. Chem Mater 25(24): 4861-4866.

Sanbonsuge S, Abe S, Handa H, Takahashi R, Imaizumi K, Fukidome H, Suemitsu M (2012) Improvement in Film Quality of Epitaxial Graphene on SiC(111)/Si(111) by SiH_4 Pretreatment. Jpn J Appl Phys 51: 06FD10.

Seo J-H, Kang B-J, Mun JH, Lim S-K, Cho BJ (2010) Effect of a surface pre-treatment on graphene growth using a SiC substrate. Microelectron Eng 87(10): 2002-2007.

Weatherup RS, Baehtz C, Dlubak B, Bayer BC, Kidambi PR, Blume R, Schloegl R, Hofmann S (2013) Introducing Carbon Diffusion Barriers for Uniform, High-Quality Graphene Growth from Solid Sources. Nano Lett 13(10): 4624-4631.

Yang H, Yan R, Chen H, Lee DH, Zheng C (2007) Characteristics of hemicellulose, cellulose and lignin pyrolysis. Fuel 86(12-13): 1781-1788.

CHAPTER IV

EFFECT OF TEMPERATURE, DURATION TIME, TEMPERATURE RISING RAMP, AND GAS FLOW RATE ON THE SYNTHESIS OF CARBONENCAPSULATED COPPER NANOPARTICLES

4.1 Introduction

Carbon encapsulated metal nanoparticles (CEMNs) have been extensively studied by scientists in the last decades due to their noble properties, and potential applications from composite products to biomedical area (Host 1998). The unique core-shell structure also enables the CEMNs be applicable in harsh environment due to the protection of carbon shells (Wu 2003). Several methods were investigated by scientists to synthesize the CEMNs, including chemical vapor deposition (Wang et al 2012), flame spray synthesis (Athanassiou et al 2006) , tungsten arc method (Host 1998), explosion method (Wu 2003), pulsed laser deposition (Wang 2013), cation exchange (Gotoh et al 2011), and thermal treatment (Mun et al 2013), etc. The phase of the raw carbon sources depended on the specific method that was applied, which could be gaseous, liquid, or solid phase. The catalyst was originated from the transition metal group. However, the synthesis mechanism has not been fully understood. There are multiple proposals by scientists based on their experiment data and results. Recently, scientists are more inclined to the dissolution-precipitation theory for metals that have large dissolution

capacity of carbon; and self-limiting theory for those have poor dissolution capacity of carbon (Zou et al 2013). We have also proposed a plastic film theory in the last Chapter.

Experiment parameters that control the synthesis process were critical to the property of final products. Nevertheless, they were not fully investigated. Temperature, gas flow, rising ramp, etc. all contributed to the quality of the synthesized products, such as thickness, number of layers, morphology, and crystallinity of graphene (Sun et al 2012).

In this study, a simple thermal treatment was applied to a mixture of pulp lignin and copper sulfate in order to synthesize carbon encapsulated copper nanoparticles (CECNs). The $L_9(3^4)$ orthogonal experiment was designed to evaluate the effect of temperature, duration time, rising ramp, and gas flow rate. X-ray diffraction spectroscopy (XRD), Scanning Electron Microscopy (SEM), Transmission Electron Microscopy (TEM), Raman spectroscopy, thermogravimetric analysis (TGA), and Fourier Transform Infrared Spectroscopy (FTIR) were utilized for characterization. The effect of each factor was discussed in details, and optimum process combination was suggested.

4.2 Material and methods

4.2.1 Synthesis of carbon encapsulated copper nanoparticles (CECNs)

The synthesis process can be referred to in Section 2.2.2. Detailed synthesis parameters are shown in Table 4.1. The purification process was referred to in Section 3.2.2. Each trial was repeated for three times.

Table 4.1 Experiment design

	FACTORS			
TRIAL #	TEMPERATURE ºC	TIME min	RAMP ºC / min	ARGON FLOW RATE sccm
OE-1	1(600)	1(30)	1(10)	1(600)
OE-2	1	2(60)	2(15)	2(1200)
OE-3	1	3(90)	3(20)	3(1800)
OE-4	2(800)	1	2	3
OE-5	2	2	3	1
OE-6	2	3	1	2
OE-7	3(1000)	1	3	2
OE-8	3	2	1	3
OE-9	3	3	2	1

4.2.2 Characterization

4.2.2.1 XRD Characterization

CECNs powder was ground and analyzed with Rigaku SmartLab X-ray diffractometer (Rigaku, Woodlands, Texas) utilizing Cu Kα radiation (λ = 1.5418 Å). The scanning range was from 10-90 °, with a scan speed of 1 °/min.

4.2.2.2 Microscopy

SEM characterization was completed on the JEOL JSM-6500F (JEOL, Peabody, Massachusetts). Sample was mounted on the carbon tape, and coated with platinum to improve its electric conductivity. TEM characterization was completed on the JOEL JEM-2100F (JEOL, Peabody, Massachusetts). Firstly the sample was dissolved in acetone and sonicated for 15 min. One drop of suspension was then dripped onto a 300 mesh copper grid with lacey carbon film (Agar Scientific, Stansted, UK), and air dried overnight before the characterization. FTIR analysis was conducted by Thermo Scientific™ Nicolet™ iS™50 FT-IR Spectrometer (Thermo Scientific, Waltham,

Massachusetts). Each spectrum was obtained in 3 s and the scanning range was from 4000 to 400 cm-1. Raman spectra were collected on the LabRAM Aramis Horiba Jobin Yvon Confocal Raman Microscope (Chicago, Illinois), with a 532 nm green laser. The scope was set at the magnification of 100X, fast mapping mode, and 4 excitement sources were used.

4.2.2.3 TGA analysis

TGA was conducted in a TGA-50H (Shimadzu, Columbia, Maryland) through isothermal analyses. The system was heated up to 700 °C at the ramping rate of 10°C/min. The change in mass was then related to the temperature changes during calcination. For each sample prepared, N_2 (99.999% purity) was flown through the TGA at 50 sccm.

4.2.3 Post thermal treatment of the synthesized CECNs

CECNs synthesized under group OE-7 were used as the raw material in this experiment. The equipment used to heat the sample was the same as that in Chapter 2, except that samples were heated in air. Three temperatures were selected (200 ºC, 300 ºC, and 500 ºC). XRD spectra and TEM graph were obtained thereafter.

4.3 Results and discussions

4.3.1 The carbonization yield

The carbonization yield was calculated in Table 4.2. There were two assumptions for the calculation:

1). There was no reaction occurred during the mixing of lignin and copper sulfate;

2). Copper element kept the same weight during the carbonization process, while sulfur and oxygen were excluded in the gaseous form from the system.

$$\text{Yield} = ((m_{ma}-m_b)-(m_{mb}-m_b)*64/416)/((m_{mb}-m_b)*256/416)*100 \quad (4.1)$$

Where m_{ma} represents the mass of the boat and sample after the thermal treatment;

m_b represents the mass of the boat;

m_{mb} represents the mass of the boat and sample before the thermal treatment;

64/416 represents the fraction of copper in the mixture;

256/416 represents the fraction of carbon source in the mixture.

Table 4.2 The yield data for different treatment groups

ID	Weight of boat 1	Weight of boat 2	Weight of boat and mixture before heating 1	Weight of boat and mixture before heating 2	Weight of boat and mixture after heating 1	Weight of boat and mixture after heating 2	Weight loss 1	Weight loss 2	yield 1	yield 2	Average
OE-1	25.18	27.35	26.70	28.88	25.85	28.03	44.00	44.69	46.50	47.63	47.06
OE-1	27.33	25.14	28.83	26.65	28.03	25.86	46.86	47.62	51.15	52.38	51.77
OE-2	27.32	25.13	28.84	26.64	28.02	25.83	45.67	46.14	49.21	49.97	49.59
OE-2	25.12	27.32	26.63	28.83	25.81	28.02	45.43	45.77	48.82	49.38	49.10
OE-3	27.32	25.13	28.83	26.64	28.00	25.82	45.06	45.67	48.23	49.22	48.72
OE-3	27.32	25.12	28.83	26.64	27.98	25.80	43.78	44.55	46.14	47.39	46.77
OE-4	25.14	27.33	26.64	28.84	25.81	28.01	45.00	45.06	48.12	48.23	48.17
OE-4	27.33	25.14	28.84	26.64	28.00	25.82	44.62	45.05	47.50	48.21	47.86
OE-5	27.32	25.12	28.83	26.63	27.96	25.78	41.98	43.56	43.22	45.78	44.50
OE-5	25.12	27.32	26.63	28.83	25.74	27.97	41.05	42.76	41.71	44.49	43.10
OE-6	27.34	25.16	28.85	26.67	28.01	25.84	44.12	45.14	46.70	48.35	47.52
OE-6	27.33	25.14	28.86	26.67	28.02	25.84	44.91	45.51	47.98	48.95	48.46
OE-7	27.32	25.12	28.83	26.63	27.98	25.79	43.71	44.03	46.02	46.55	46.29
OE-7	27.32	25.12	28.83	26.63	27.98	25.79	43.97	44.45	46.46	47.23	46.84
OE-8	25.15	27.34	26.67	28.86	25.83	28.01	44.27	44.33	46.93	47.04	46.98
OE-8	25.14	27.33	26.65	28.85	25.81	28.00	43.84	43.93	46.24	46.39	46.31
OE-9	25.13	27.33	26.64	28.84	25.80	28.00	44.28	44.57	46.95	47.42	47.19
OE-9	25.13	27.33	26.64	28.83	25.79	27.99	43.79	44.04	46.16	46.57	46.36

The carbonization yield for all groups ranged between 43% and 50%. Figure 4.1 shows that the yield decreased with the increase of temperature, except for group OE-5. Heat would facilitate the decomposition of lignin and generate more gas. At low and medium temperature range (600 °C and 800 °C), other parameters also contribute to affect the yield. Medium duration time (60 min), fast ramp (20 °C/min), and low flow rate of argon gas (600 sccm) were favorable for the decomposition of lignin. However, at high temperature (1000 °C), the yield was almost the same, no matter what other parameters were.

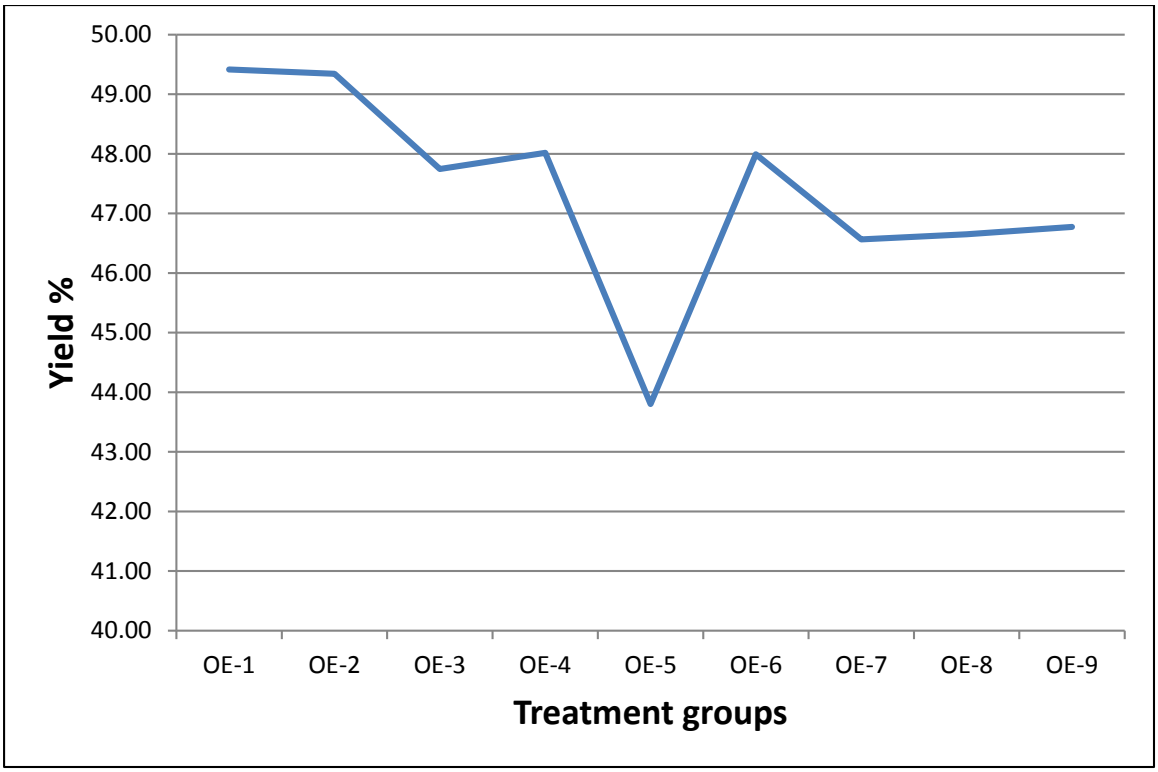

Figure 4.1 Trend of yield for different treatment groups

4.3.2 X-ray diffraction spectra

Figure 4.2 shows the X-ray diffraction spectra of HNO_3 purified CECNs for all 9 treatment groups. There is a broad peak at 2θ =24 °, which was a fitted peak for both graphite (0 0 2) at approximately 2θ =26.2 ° (Ou et al 2008) and amorphous carbon at 2θ =20-27 °. Figure 4.2 reveals that with the increase of temperature, the peak at 2θ =24 ° became sharper, indicating higher crystallinity of the sample. Gaussian function was applied to fit the curve. The crystallinity was calculated as

$$W_c = \frac{A_c}{A_c + A_a} \tag{4.2}$$

Where the peaks of graphite at 2θ =26.2 °, 42.2 °, and 46.4 ° were categorized as the crystalline region, denominated as A_c, while the rest of the carbon peaks were categorized as the amorphous one, denominated as A_a. Results are shown in Table 4.3. Data in each cell of rows I, II, and III originate from a summation of crystallinity in respective level (I, II, or III) within each factor. For example, the datum in the row level II, column 3 (9.95) is the sum of crystallinity in all three level IIs within the column of factor time (row OE-2, OE-5, and OE-8), which equals to 2.44 +2.68 + 4.83= 9.95. K_1, K_2, and K_3 are the one third of corresponding I, II, and III, respectively. R is the difference between the maximum and minimum K value in each column. Higher R value indicates more importance of that specific factor on the crystallinity of the CECNs.

Temperature was the most important factor that affected the crystallinity, with the highest R value of 3.85. The crystallinity went higher with the increase of temperature. Graphene is made of C=C bonds. The bond energy of C-C bond is 347 kJ / mol, and that of C=C bond is 614 kJ/mol (Tarendash 2006). High temperature provided more possibility of converting C-C bond into C=C bonds, thus increasing the crystallinity of the final products. The second important factor was the argon flow rate. Medium flow rate was favorable, too fast or too slow would impact the gaseous carbon deposition on the copper surface. We proposed the synthesis mechanism in Chapter III, which stated that gaseous carbon did not help in the graphene growth process due to limited amount of gaseous carbon at the critical temperature. Appropriate amount of carbon atoms were required for the graphene growth: fast gas flow rate resulted in few available carbon atoms; slow gas flow rate generated excessive carbon atoms deposited on the surface of copper

nanoparticles, which passivated the surface, and increased the amount of amorphous carbon (Chen and Hsieh 2014).

Duration time had less impact on the crystallinity. Results indicated that short duration time was preferred. There might be side reactions on the final products if the duration time was long, introducing more defects, as suggested by Chae et al (2009). The least important factor was the temperature rising ramp. Data showed that the faster the ramp was, the higher the crystallinity was. This agreed with the short duration time theory: fast temperature rising ramp equals to that sample was heated up to a specific temperature quickly, so that overall the sample had a short exposing time to heat. The optimum combination of the synthesis parameters was 1000 °C, 30 min duration time, 20 °C/min temperature rising ramp, and 1200 sccm gas flow rate.

Table 4.3 Crystallinity results

	FACTORS				
TRIAL #	TEMPERATURE ºC	TIME min	RAMP ºC/min	ARGON FLOW RATE sccm	Crystallinity %
OE-1	1(600)	1(30)	1(10)	1(600)	0.44
OE-2	1	2(60)	2(15)	2(1200)	2.44
OE-3	1	3(90)	3(20)	3(1800)	1.47
OE-4	2(800)	1	2	3	4.12
OE-5	2	2	3	1	2.68
OE-6	2	3	1	2	2.5
OE-7	3(1000)	1	3	2	8.73
OE-8	3	2	1	3	4.83
OE-9	3	3	2	1	2.33
I	4.35	13.29	7.77	5.45	
II	9.30	9.95	8.89	13.67	
III	15.89	6.30	12.88	10.42	
K_1	1.45	4.43	2.59	1.82	T=29.54
K_2	3.10	3.32	2.96	4.56	
K_3	5.30	2.10	4.29	3.47	
R	3.85	2.33	1.70	2.74	

The sharp peak at 2θ =43.3 ° was assigned to element Cu (111) (Huang et al 2009), indicating that the Cu^{2+} was reduced to zero valence during the thermal treatment. Copper nanoparticles heated at 600 °C were washed out after HNO_3 purification, implying that the copper nanoparticles were not flawlessly encapsulated by the graphene layers, similar to that at lower temperature range (300 °C -500 °C). The perfectness of the shell was correlated with the heating temperature: the higher the temperature, the shaper the peak of Cu (111) was found, which was equivalent to that the graphene layers had fewer defects. At 1000 °C, there was not much difference in the leaching of copper nanoparticles, since the intensity of the peak of Cu (111) was about the same, no matter

what the duration time, ramp, and gas flow rate were, similar results were found with the carbonization yield at 1000 °C.

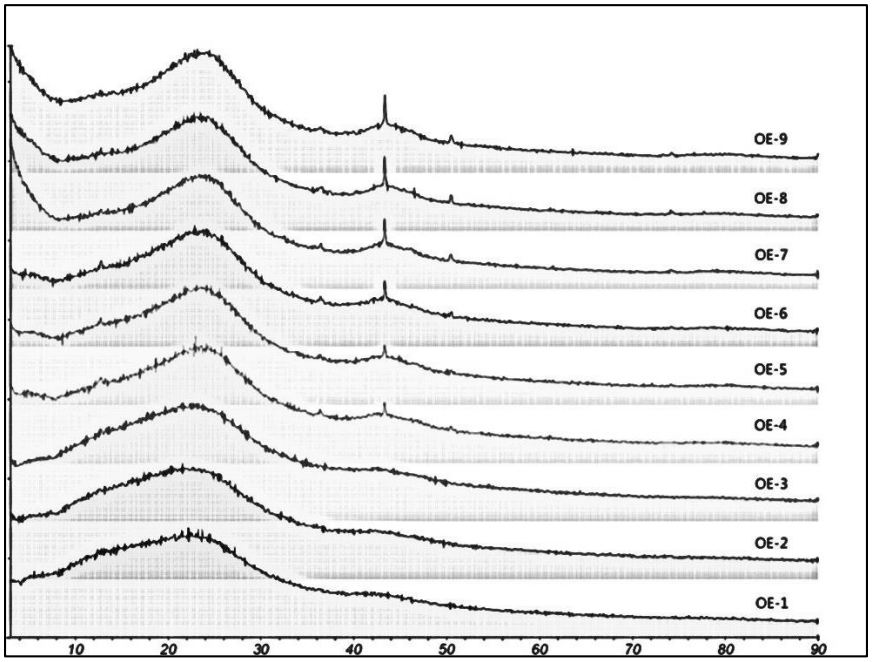

Figure 4.2 X-ray diffraction spectra of HNO_3 purified CECNs (OE-1 to OE-9)

4.3.3 FTIR spectra

Figure 4.3 shows the FTIR spectra of the raw BCL-DI lignin and sample treated at all nine groups. In the typical BCL-DI lignin spectrum, the peak at around 3450 cm^{-1} represents the O-H stretch. The one at 2900 cm^{-1} is the C-H stretch; the one at 2260 cm^{-1} is the typical C≡C stretch. In the fingerprint region, the peaks at 1700 cm^{-1} and 1230 cm^{-1} are representative of C=O stretches. Both peaks at around 1600 cm^{-1} and 1500 cm^{-1} are characteristic for aromatic C=C ring vibration, which is the basic skeleton of lignin (Zhou et al 2011). The peaks at 1450 cm^{-1}, 1420 cm^{-1}, 1200 cm^{-1}, and 800 cm^{-1} indicate the C-H deformation, of which, the one at 1450 cm^{-1} is from methylene C-H bend, the one at 1420

cm^{-1} is assigned for vinyl C-H in plane bend, the one at 1200 cm^{-1} is the aromatic C-H in plane bend, while the one at 800 cm^{-1} is the aromatic C-H out of plane bend. The peaks at 1250 cm^{-1} and 1050 cm^{-1} represent the aromatic O-H stretch and alkyl-substituted C-O-C stretch, respectively. C-C skeletal vibration is shown at 1150 cm^{-1} (Coates 2000).

Spectra of sample treated at 600 ºC were slightly different from that treated at higher temperature, with sharper peaks of C=O, aromatic C=C, and aromatic C-H bonds showing at 1700 cm^{-1}, 1500 cm^{-1}, and 700-900 cm^{-1}, respectively. The C≡C peak at 2260 cm^{-1} did not change for all treatment combinations. C=O bond was the main source that would be converted into CO and CO_2 gas by annealing. However, for lignin, the converting temperature from C=O bond to gas was higher than 600 ºC (Yang et al 2007), which was the reason that there still was a C=O peak in the spectrum collected at 600 ºC. The aromatic C=C bond at around 1600 cm^{-1} was stable during mild annealing conditions. With the increase of temperature, the intensity of C=C peak continued to decrease.

The peak of O-CH_3 was at the similar wavenumber as that of C=C. However, in this spectrum, we considered there was only C=C peak, since that O-CH_3 started to convert into CH_4 at low temperature from 280 ºC to 520 ºC (Yang et al 2007), which should be excluded from the system at the higher temperature range.

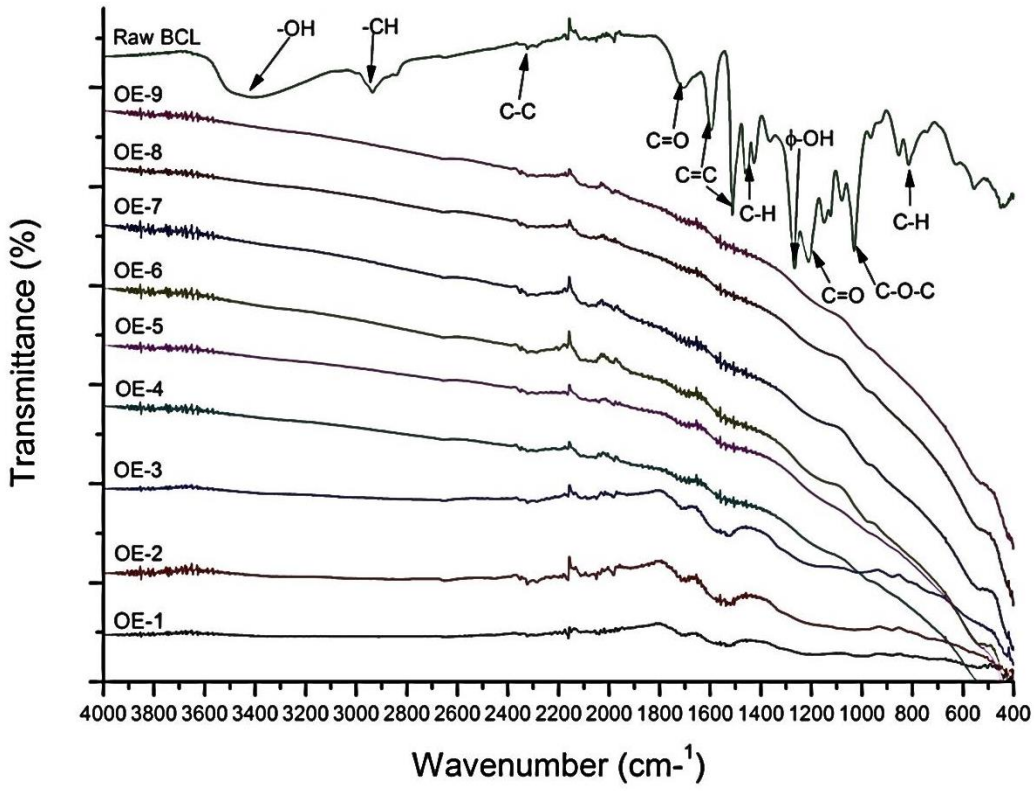

Figure 4.3 FTIR spectra (Raw BCL-DI lignin and groups OE-1 to OE-9)

4.3.4 Electron microscope characterization

It was still not easy to locate the graphene structure under TEM when the sample was heat treated at low temperature (600 ºC). The graphene layer was disordered, and only a few copper nanoparticles that were shelled with graphene were located. As exposed to heat for longer time, higher temperature rising ramp, and faster gas flow rate, it was easier to locate the graphene layers, some of which were netted with others and formed complicate structures.

With the increase of temperature (600 ºC → 800 ºC → 1000 ºC), there were more graphene encapsulated copper nanoparticles found under the microscope. Especially for

the sample treated at 1000 ºC, large number of copper nanoparticles shelled with graphene layers were found, and several empty graphene shells were also shown in Figure 4.4. The number of graphene layers was around 2 to 3, which was smaller than those treated at 400 ºC and 500 ºC in Chapter 3, and also smaller than those treated with active transition metals such as iron, nickel, cobalt, etc. The difference in the number of graphene layers was due to fundamental growth mechanism (Zou et al 2013). The graphene growth mechanism was discussed in Chapter 3. Higher temperature could remove the amorphous carbon covered on the surface of graphene, and redefine the flaw graphene grown at low temperature.

Compared with iron, copper has poor dissolving capacity of carbon, the plastic lignin film could barely be dissolved into copper atoms, while only cover the surface of copper nanoparticles and isolate any other contact. The low dissolving capacity has limited the number of graphene layers that could be synthesized.

As for the gaseous carbon source such as CH_4, it was generated at a wide range of temperature (Yang et al 2007), which would be deposited on the available surface of copper nanoparticles and grew into graphene.

Figure 4.4 shows that the size of the copper nanoparticles and the empty graphene shells was around 10 nm, which was promising in some applications, for example, wood preservation. The size of preservative should be smaller than the size of pits in order to pass through and arrive to the target cell wall. Other applications that needed larger particle size could be achieved by using other forms of carbon sources and catalysts.

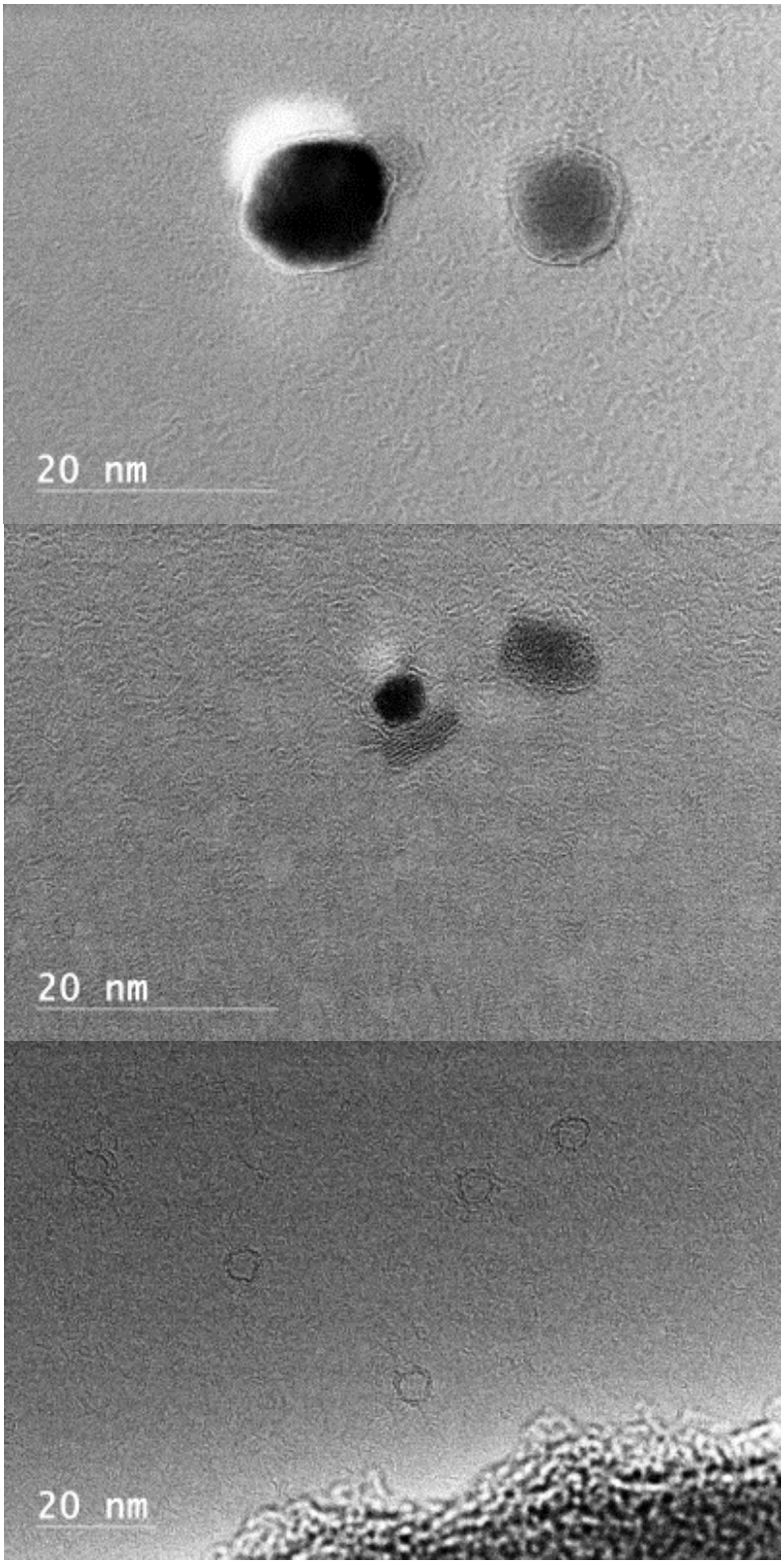

Figure 4.4 TEM photos of HNO_3 purified CECNs

4.3.5 Raman spectra

Raman Spectra for samples treated at groups 1, 4, and 7 are shown in Figure 4.5. There is a peak at around 1350 cm^{-1}, which was known as the D peak. D peak was reflected by the defective sites which might be caused by the disordered sp^2 carbon configuration or curvature strain (Lee et al 2013). There is another peak at about 1590 cm^{-1}, knows as the G peak, which was indicated as the graphene layer. The ratio of I_D/I_G was used to evaluate the perfectness of CECNs synthesized. We can conclude from Table 4.4 that for all the three treatment groups, the degree of defect was reduced after HNO_3 purification. HNO_3 acted as a cleaner to get rid of excessive amorphous carbon, hence the intensity of D peak reduced.

Table 4.4 also shows that the sample treated at 800 ºC has the least I_D/I_G ratio, which was not in consistence with the XRD result. It was supposed that the defect of the CECNs be less at higher temperature. The reason for the contradiction might be originated from the size of laser beam and the sensitivity of the Raman spectrometry, which recognized more area as the defect region.

Less intensity was recorded at higher temperature, as shown in Figure 4.5. In fact, the absolute intensity is proportionate to the amount of material under the scope: more scatters will be obtained if there is larger amount of samples under the scope. The absolute intensity has little meaning, while the ratio of I_D/I_G does.

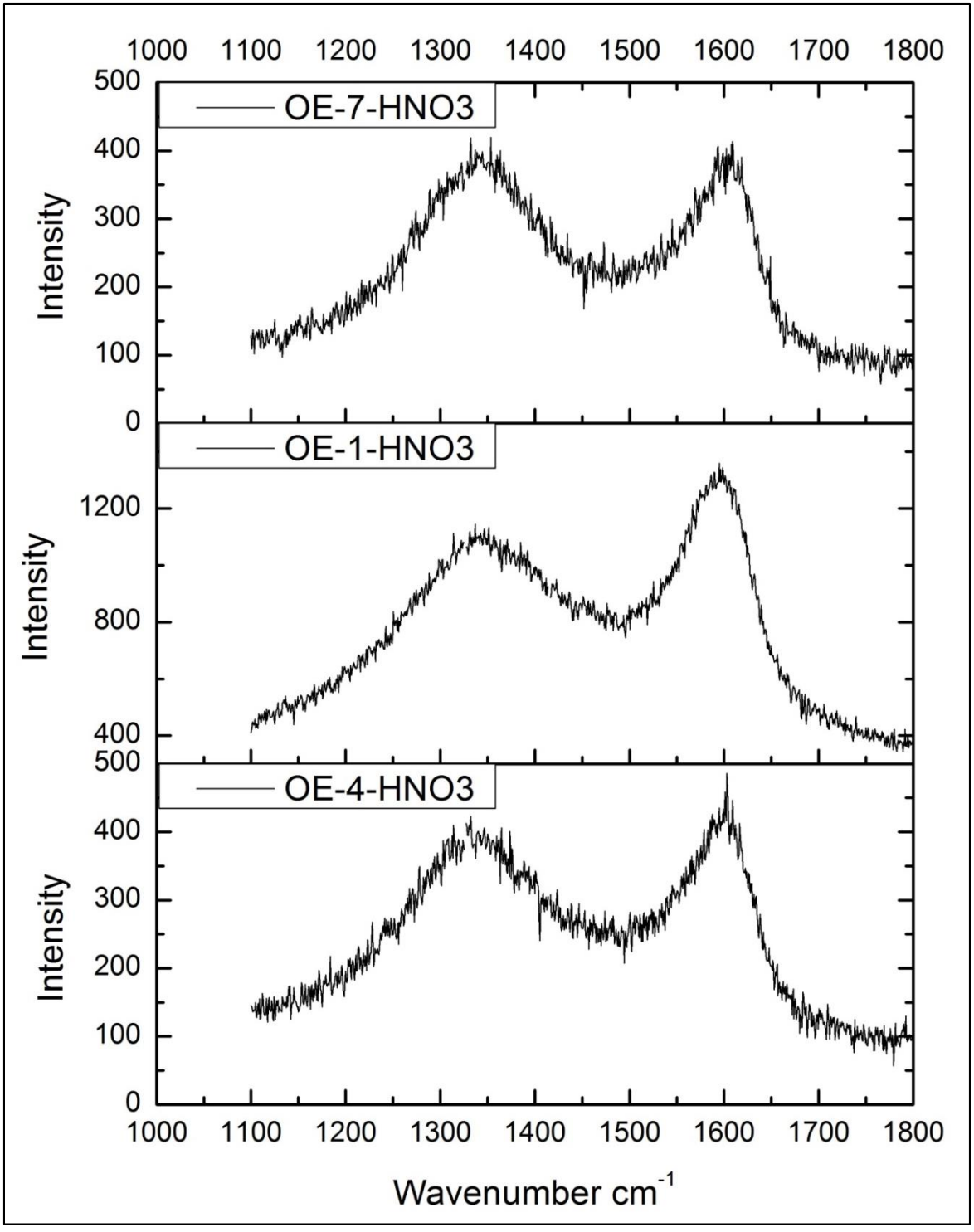

Figure 4.5 Raman spectra (OE-1, OE-4, and OE-7 after HNO_3 purification)

Table 4.4 Ratio of I_D/I_G

OE-1	1956.73	2453.60	0.88
OE-1-HNO_3	1112.62	1271.41	0.88
OE-4	429.64	433.54	0.99
OE-4-HNO_3	412.59	486.11	0.85
OE-7	546.33	516.25	1.06
OE-7-HNO_3	383.10	413.76	0.93

4.3.6 TGA analysis

The TGA analysis results were shown in Figure 4.6. There was a slight weight loss at 100 ºC for all samples, which was believed to be caused by the evaporation of H_2O. Then the curve was gradual for each sample until an abrupt weigh loss occurred at above 300 ºC.

Sample treated with 600 ºC, 30 min, 10 ºC/min, and 600 sccm started to have an sudden weight loss from 350 ºC, and ended at 430 ºC, indicating that this sample had the worst thermal stability. Sample treated with 800 ºC, 30 min, 15 ºC/min, and 1800 sccm resulted in better thermal stability, with an abrupt weight loss starting from 400 ºC, and ending at above 500 ºC. Sample treated with 1000 ºC, 30 min, 20 ºC/min, 1200 sccm, and 1000 ºC, 90 min, 15 ºC/min, 600 sccm had similar weight loss curves, and these two groups presented the best thermal stability, which started to have a great weight loss from 450 ºC, while ended at above 600 ºC, and the slope was much flatter than the other two curves. Results also implied that temperature was a more important factor than the others.

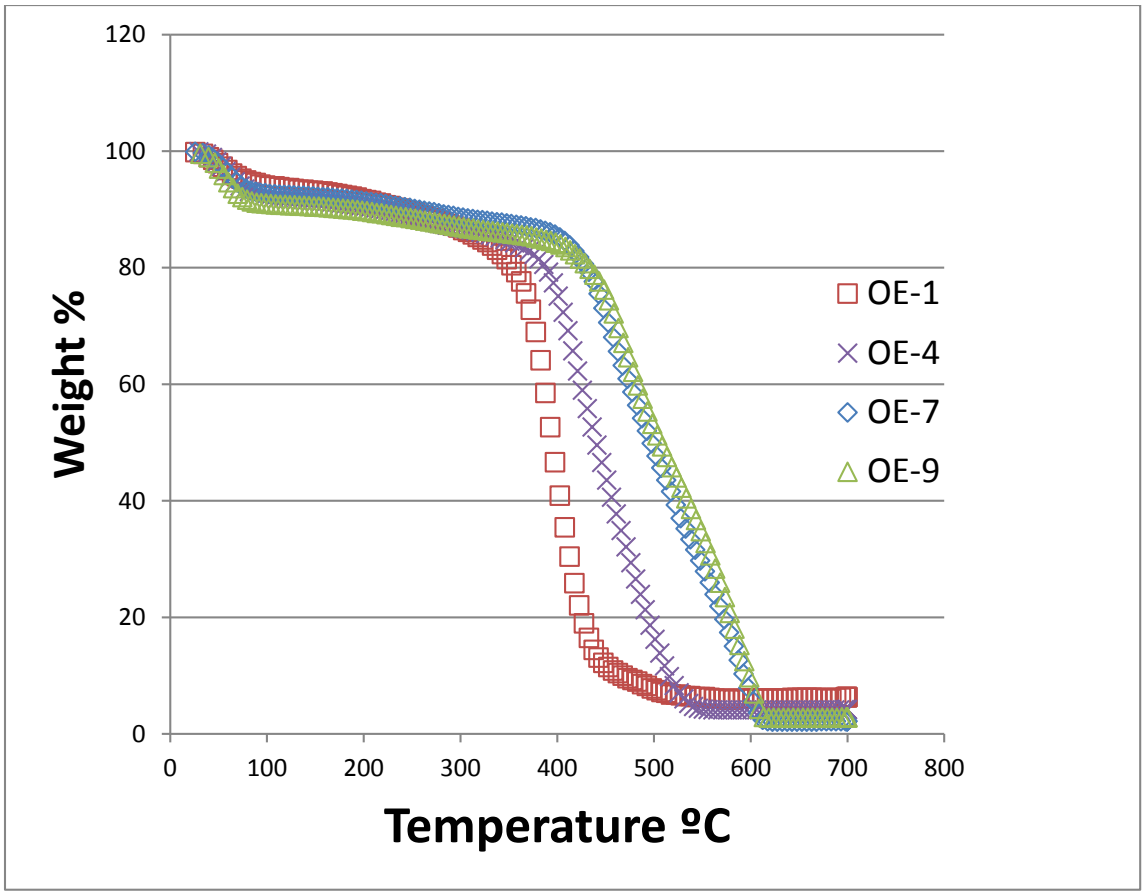

Figure 4.6 TGA analysis graph for samples treated with parameter groups 1, 4, 7, and 9

4.3.7 The effect of post heat treatment on the crystallinity of graphite

Table 4.5 shows the weight loss of CECNs post heated at 200 ºC, 300 ºC, and 500 ºC, respectively. CECNs were stable during post heat treatment at 200 ºC, with the weight loss of 3.99%. The weight loss was attributed to water vaporization, and no oxidation reaction occurred. When post heated at 300 ºC, the weight loss increased suddenly to 35.54%. Amorphous carbon was believed to burn into gas and contribute mainly to the weight loss. Further increase the temperature up to 500 ºC resulted in 91.43% weight loss. At this point, all amorphous carbon might be gone or reconfigured.

Copper nanoparticles might also be changed into other forms. Otherwise, the weight loss should not be over 90%. Further study needs to be continued.

Table 4.5 Yield of CECNs post heated at 200 ºC, 300 ºC, and 500 ºC

Sample ID	Weight loss %
OE-7-200	3.99
OE-7-300	35.54
OE-7-500	91.43

The change of graphite and copper is illustrated in the XRD spectra (Figure 4.7). CECNs post heated at 200 ºC showed almost no changes in copper and graphite peaks; for that post heated at 300 ºC, the intensity of Cu_2O peak at around 37 º was strengthened, and the intensity of Cu peak decreased. However, the improvement of graphite crystallinity could not be determined; further increase the temperature to 500 ºC resulted in almost complete oxidation of Cu atoms and the formation of Cu_2O and CuO. A sharp graphite peak appears at around $2\theta = 26$ º for the CECNs post heated at 500 ºC, which means that the crystallinity was improved after the post thermal treatment. The graphite peak was shifted to the right with the increase of post heat temperature, and finally close to $2\theta = 26$ º. Research has proved that graphene was stable, no changes occurred even under thermal treatment (Hsieh et al 2013). The improvement of graphite should be contributed by the decrease of amorphous carbon.

Figure 4.8 shows the morphology of sample post heated at 500 ºC. More graphene bands were obtained after the thermal oxidation. Part of the amorphous carbon was burned into gas, and part of them was transformed into graphene structures.

Post heat treatment was proved to be a feasible way to improve the crystallinity of the graphite.

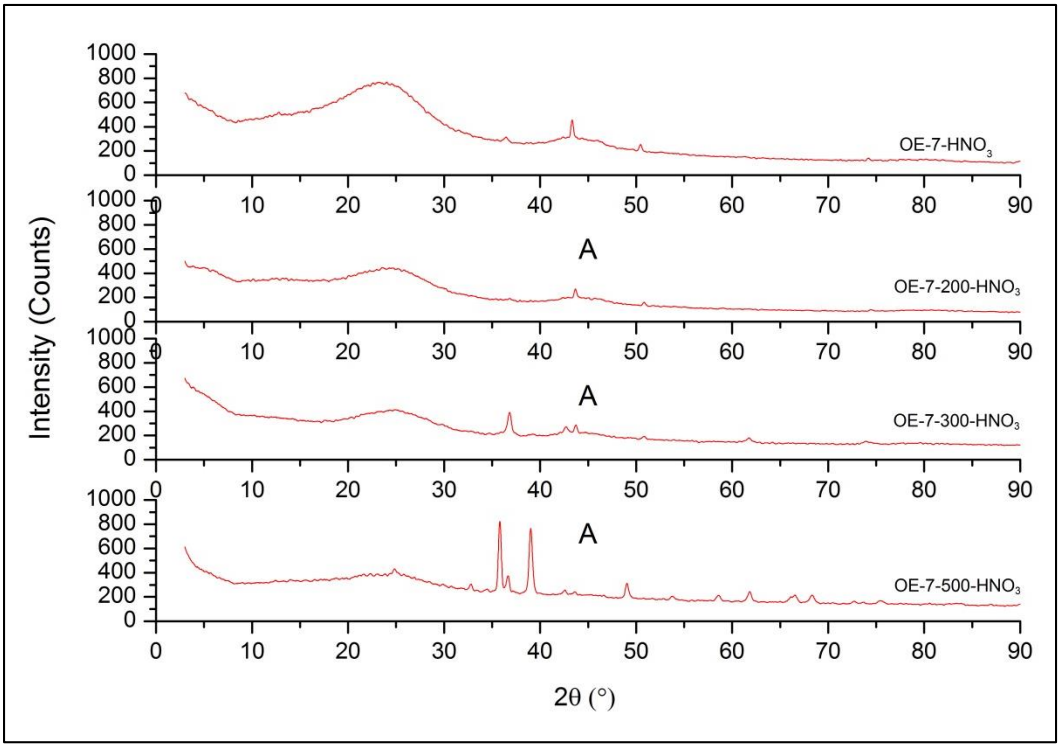

Figure 4.7 XRD spectra of the CECNs treated at 1000 ºC, 30 min, 20 ºC/min, and 1200 sccm gas flow rate, and the same CECNs post heated at 200 ºC, 300 ºC, and 500 ºC in air

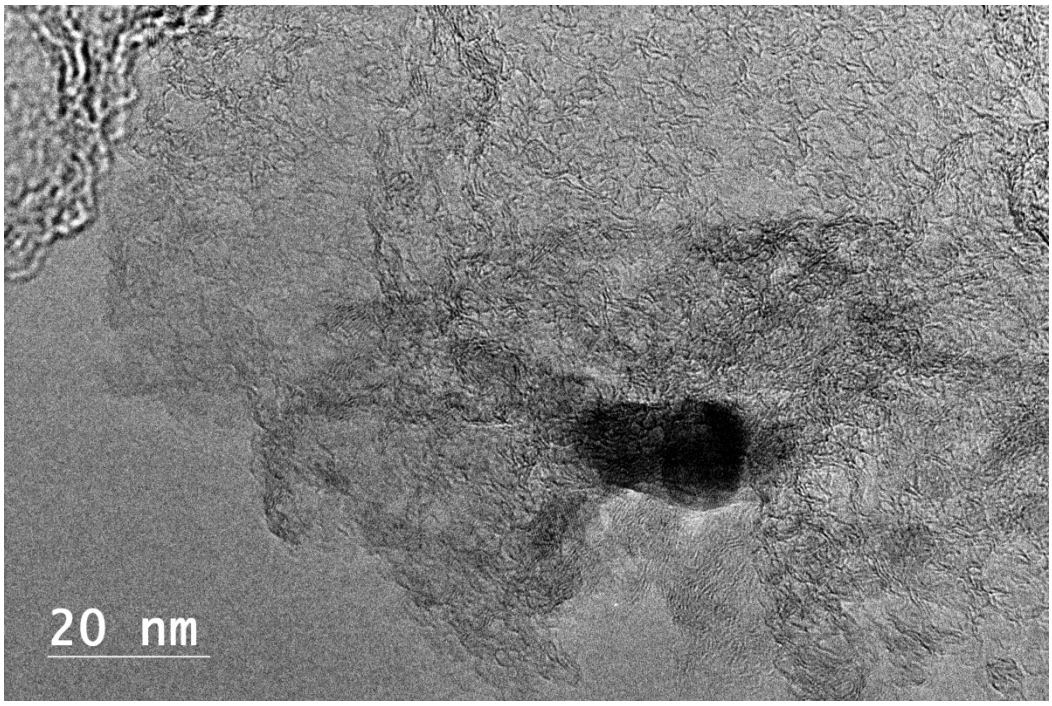

Figure 4.8 TEM image of CECNs post heated at 500 ºC in air

4.4 Conclusion

The orthogonal experiment design was applied to characterize the synthesized carbon encapsulated copper nanoparticles. In this study, XRD, SEM, TEM, FTIR, and RAMAN Spectroscope were utilized. Results revealed that temperature played the most important role in the growth of graphene: high temperature was preferred in order to obtain less defect sites. Complicate reactions existed during the annealing process. The optimum synthesis parameters were suggested as 1000 °C, 30 min duration time, 20 °C/min temperature rising ramp, and 1200 sccm argon gas flow rate. Post heat treatment was proved to be a feasible way to improve the crystallinity of graphite.

4.5 References

Athanassiou EK, Grass RN, Stark WJ (2006) Large-scale production of carbon-coated copper nanoparticles for sensor applications. Nanotechnol 17(6): 1668-1673.

Chae SJ, Günes, F, im KK, Kim ES, Han GH, Kim SM, Shin H-J, Yoon S-M, Choi J-Y, Park MH, Yang CW, Pribat D, Lee YH (2009) Synthesis of Large-Area Graphene Layers on Poly-Nickel Substrate by Chemical Vapor Deposition: Wrinkle Formation. Adv Mater 21(22): 2328-2333.

Chen C-S, Hsieh C-K (2014) Effects of acetylene flow rate and processing temperature on graphene films grown by thermal chemical vapor deposition. Thin Solid Films In press.

Coates J. (2000). Interpretation of Infrared Spectra, A Practical Approach. John Wiley & Sons Ltd, Chichesterpp.

Gotoh K, Kinumoto T, Fujii E, Yamamoto A, Hashimoto H, Ohkubo T, Itadani A, Kuroda Y, Ishida H (2011) Exfoliated graphene sheets decorated with metal/metal oxide nanoparticles: Simple preparation from cation exchanged graphite oxide. Carbon 49(4): 1118-1125.

Host JJaD, Vinayak P and Teng, Mao-Hua (1998) Systematic study of graphite encapsulated nickel nanocrystal synthesis with formation mechanism implications. J Mater Res 13(09): 2547--2555.

Hsieh Y-P, Wang Y-W, Ting C-C, Wang H-C, Chen K-Y, Yang C-C (2013) Effect of Catalyst Morphology on the Quality of CVD Grown Graphene. J Nanomater 2013: 1-6.

Huang C-H, Wang HP, Chang J-E, Eyring EM (2009) Synthesis of nanosize-controllable copper and its alloys in carbon shells. Chem Commun(31): 4663.

Lee S, Hong J, Koo JH, Lee H, Lee S, Choi T, Jung H, Koo B, Park J, Kim H, Kim Y-W, Lee T (2013) Synthesis of Few-Layered Graphene Nanoballs with Copper Cores Using Solid Carbon Source. ACS Appl Mater Interf 5(7): 2432-2437.

Mun SP, Cai Z, Zhang J (2013) Fe-catalyzed thermal conversion of sodium lignosulfonate to graphene. Mater Lett 100: 180-183.

Ou Q, Tanaka T, Mesko M, Ogino A, Nagatsu M (2008) Characteristics of graphene-layer encapsulated nanoparticles fabricated using laser ablation method. Diam Relat Mater 17(4-5): 664-668.

Sun Z, Raji A-RO, Zhu Y, Xiang C, Yan Z, Kittrell C, Samuel E, Tour JM (2012) Large-Area Bernal-Stacked Bi-, Tri-, and Tetralayer Graphene. ACS nano 6(11): 9790--9796.

Tarendash AS. (2006). Let's Review Chemistry: The Physical Setting (4th ed.). New York: Library of Congress Cataloging-in-Publication Datapp.

Wang K. (2013) Laser based fabrication of graphene, advances in graphene science, In Aliofkhazraei M (Ed.) Advances in graphene science. Intech.

Wang S, Huang X, He Y, Huang H, Wu Y, Hou L, Liu X, Yang T, Zou J, Huang B (2012) Synthesis, growth mechanism and thermal stability of copper nanoparticles encapsulated by multi-layer graphene. Carbon 50(6): 2119-2125.

Wu WaZ, Zhenping and Liu, Zhenyu and Xie, Yaning and Zhang, Jing and Hu, Tiandou (2003) Preparation of carbon-encapsulated iron carbide nanoparticles by an explosion method. Carbon 41(2): 317--321.

Yang H, Yan R, Chen H, Lee DH, Zheng C (2007) Characteristics of hemicellulose, cellulose and lignin pyrolysis. Fuel 86(12-13): 1781-1788.

Zhou G, Taylor G, Polle A (2011) FTIR-ATR-based prediction and modelling of lignin and energy contents reveals independent intra-specific variation of these traits in bioenergy poplars. Plant Methods 7(1): 9.

Zou Z, Dai B, Liu Z (2013) CVD process engineering for designed growth of graphene. Sci Sin Chim 43(1): 1.

CHAPTER V

FUNCTIONALIZATION OF CARBON ENCAPSULATED COPPER NANOPARTICLES WITH ORGANIC CHEMICALS

5.1 Introduction

Graphene is a zero band gap material. The inertness of sp^2 hybridized carbon organized graphene has hindered its application (Woszczyna et al 2014). Functionalization is a promising path to open the band gap and to broaden the application of graphene. Graphene attached with different functional groups could be used in mechanical engineering (Liu et al 2014), electrical device (Jokar et al 2014b), aerospace engineering (Yi et al 2013), bio-medicine (Xu et al 2014), antibacterial (Nam et al 2013),etc.

Functionalization could be achieved by chemical, electrochemical reactions, radical reaction, π-π stacking, etc. Each method has its merits and demerits.

Chemical oxidation was widely used to attach various functional groups onto the graphene edge and surface. Oxygen containing groups were introduced to the graphene layers, and acted as the nucleation sites, which were ready to be linked with external material (Jokar et al 2014a). However, the entrance of oxygen groups altered the structure of graphene, thus the property changed far away from its origin. More defects were also generated (Boukhvalov and Katsnelson 2008). Several methods were studied in order to

address these issues. Reduction of chemical oxidized graphene was a popular way to maintain the oxygen containing groups on graphene without big change of the property (Bjerglund et al 2014). Utilizing organic compounds in the oxidation was another way to reduce damage to the graphene property, specifically the π conjugation (Yang and He 2014).

Non-covalent π-π stacking was an alternative to protect the pristine graphene property (Hamilton 2009). Instead of making covalent bond, π-π stacking of functional groups into graphene through van der Waals forces was much easier (Woszczyna et al 2014). The weak van der Waals forces between functional groups and graphene could result in homogeneous dispersion (Wei and Qiu 2014). However, in harsh condition, graphene agglomeration could occur.

The combination of covalent and non-covalent functionalization was often conducted to conquer these shortcomings (Roppolo et al 2014), which, for example, was successfully adopted in biomedical application: the covalent amidation of graphene oxide with polyethylene glycol, followed by non-covalent π-π stacking of paclitaxel made it work for cancer chemotherapy(Xu et al 2014).

Electrochemical functionalization was intensively investigated as it had many advantages. Electric reaction charged the graphene, and made it easy to connect with opposite charged functional groups (Vu et al 2014). Nitrogen, chlorine, and fluorine were often used in the electrochemical functionalization. The property of nitrogen was similar to carbon as it was next to carbon in the periodic table (Kaur et al 2015). The reaction between chlorine and graphene was sensitive to the DC voltage bias, which could be engineered to obtain different products (Zhang et al 2013). Fluorine was very reactive,

and it started to react with graphene at the defective sites and edges, which could improve the quality of graphene and make it more stable (Nebogatikova et al 2014).

Electrochemical functionalization was usually used in the electronics and battery industry such as super-capacitance (Shruthi et al 2014). The addition of functional groups made the planar space of graphene larger, hence increased the electron storage capacity (Ebrish et al 2014).

The functionalization performance was affected by many factors, such as the size of the functional groups (Jang et al 2014; Wang et al 2014), morphology (Ensafi et al 2014), voltage (Byun et al 2014), steric limitation (Nguyen et al 2014), etc. 3D graphene showed better properties than the 2D counterpart in mechanical strength, electron and mass transfer (Liu et al 2014). Asymmetric functionalization for the two surfaces of graphene could lead to an increase in the reactivity as the electronic structure was different for each side (Bissett et al 2014).

In this study, the organic chemical functionalization of previously synthesized CECNs was studied. Morphology and spectra characterization were discussed in details.

5.2 Material and methods

5.2.1 Functionalization of CECNs

HNO_3 purified CECNs were used as the raw material, which had poor solubility in water and other solvent such as acetone, ethanol. N-methyl-2-pyrrolidone (NMP) (anhydrous, 99.5%), polyvinylpyrrolidone (PVP) (average mol wt 40,000), and toluene (anhydrous, 99.8%) were purchased from Sigma Aldrich (St. Louis, Missouri, USA). All chemicals were used as received.

In this study, 2.5 g HNO_3 purified CECNs were added into a 100 mL conic flask. 26 mL of NMP and 18 mL of toluene were mixed into the conic flask, followed by 3h continuous sonication. The mixture was then through centrifugation at a rate of 4000 rmp for 20 min in a Fisher Scientific™ accuSpin™ 3R centrifuge (Waltham, Massachusetts, USA). The mixture was separated into two phases after the centrifugation, as shown in Figure 5.1a. The upper phase was extracted with pipette and ready for subsequent experiment.

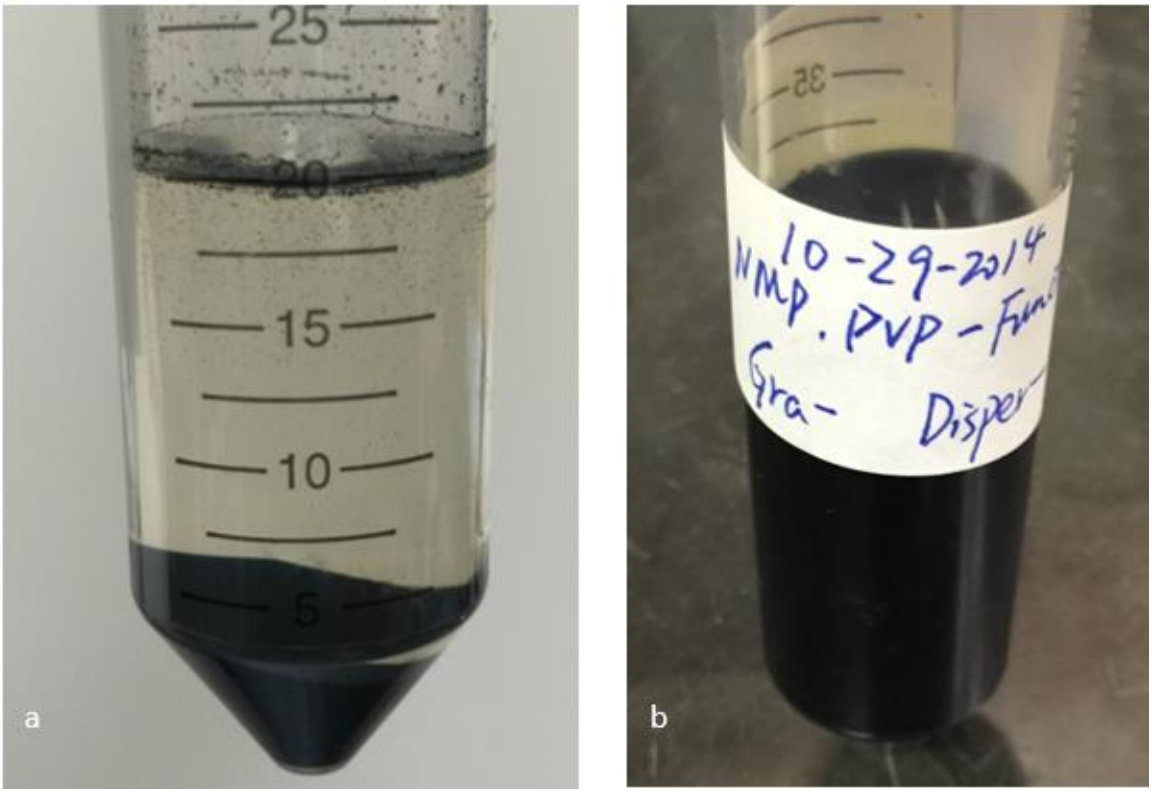

Figure 5.1 CECNs samples treated with NMP, toluene, and PVP

a: The mixture of CECNs, NMP, and toluene after centrifugation
b: Homogeneous solution of PVP, NMP-functionalized CECNs

The leftovers of the previous mixture were transferred into a 150 mL conic flask, followed by the addition of 9 mg of PVP and 86 mL of NMP. The new mixture was sonicated for another 6 h and then centrifuged at the same rate and time. Finally, a homogeneous solution was obtained (Figure 5.1b). The functionalized CECNs were able to be dissolved into H_2O and ethanol and resulted in a homogeneous solution.

5.2.2 FTIR and TEM characterization

FTIR analysis was conducted by the Thermo Scientific™ Nicolet™ iS™50 FT-IR Spectrometer (Thermo Scientific, Waltham, Massachusetts). Background was collected first. Then one drop of the homogeneous solution was dripped right onto the slit. No pressure was needed for liquid sample. Each spectrum was obtained in 3 s and the scanning range was from 4000 cm^{-1} to 400 cm^{-1}.

TEM characterization was completed on the JOEL JEM-2100F (JEOL, Peabody, Massachusetts). One drop of the homogeneous solution was dripped onto a 300 mesh copper grid with lacey carbon film (Agar Scientific, Stansted, UK), then it was air dried overnight before the characterization.

5.3 Results and discussion

5.3.1 FTIR characterization

The FTIR spectrum of PVP, NMP-functionalized CECNs is shown in Figure 5.2. Only the region from 2000 cm^{-1} to 500 cm^{-1} was illustrated, since this region was characteristic for the identification of functionalization performance. The sharp peak at around 1660 cm^{-1} is characteristic for the C=O bond of PVP and NMP (Arsalani et al 2010; Geng et al 1997; Laot et al 1999; Saravanan et al 2011; Tu et al 2008). The

aromatic C=C bond at 1500 cm^{-1} confirmed the existence of toluene. The scissoring bending of cyclic C-H is shown at 1460 cm^{-1} and 1420 cm^{-1} (Arsalani et al 2010; Laot et al 1999). The O-H bending from hydroxyl groups is shown at 1400 cm^{-1} (Fernandez-Merino et al 2010). The three sharp peaks at 1290 cm^{-1}, 1250 cm^{-1}, and 1110 cm^{-1} are assigned to C-N stretching bond of PVP and NMP (Arsalani et al 2010; Gardolinski et al 1999; Giri et al 2011; Saravanan et al 2011). In addition, the two amide V and IV bands at 730 cm^{-1} and 650 cm^{-1} confirmed the covalent linkages between CECNs and PVP and NMP (Laot et al 1999). The two peaks at 1220 cm^{-1} and 980 cm^{-1} are characteristic for the C-O-C bond.

FTIR spectrum successfully proved the feasibility of NMP, PVP functionalization, and made it possible for further modification of CECNs.

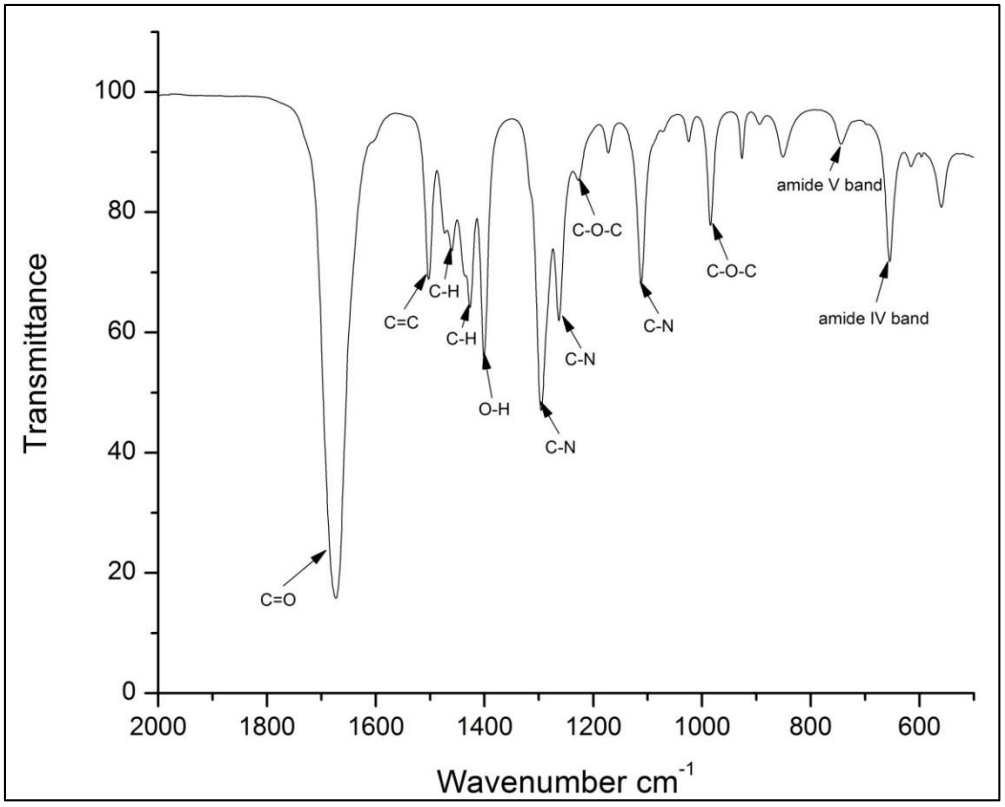

Figure 5.2 FTIR spectra of PVP, NMP-functionalized CECNs

Wavenumber from 2000 cm^{-1} to 500 cm^{-1}

5.3.2 TEM characterization

The dispersion of NMP, PVP functionalized CECNs was observed by TEM. The functionalized nanoparticles were uniformly dispersed in toluene solvent (Figure 5.3a). TEM image also shows that copper atoms were further removed during the sonication and centrifugal process, with increasing amount of empty graphene shells showing in Figure 5.3b. This structure could be beneficial in some applications of the functionalized CECNs.

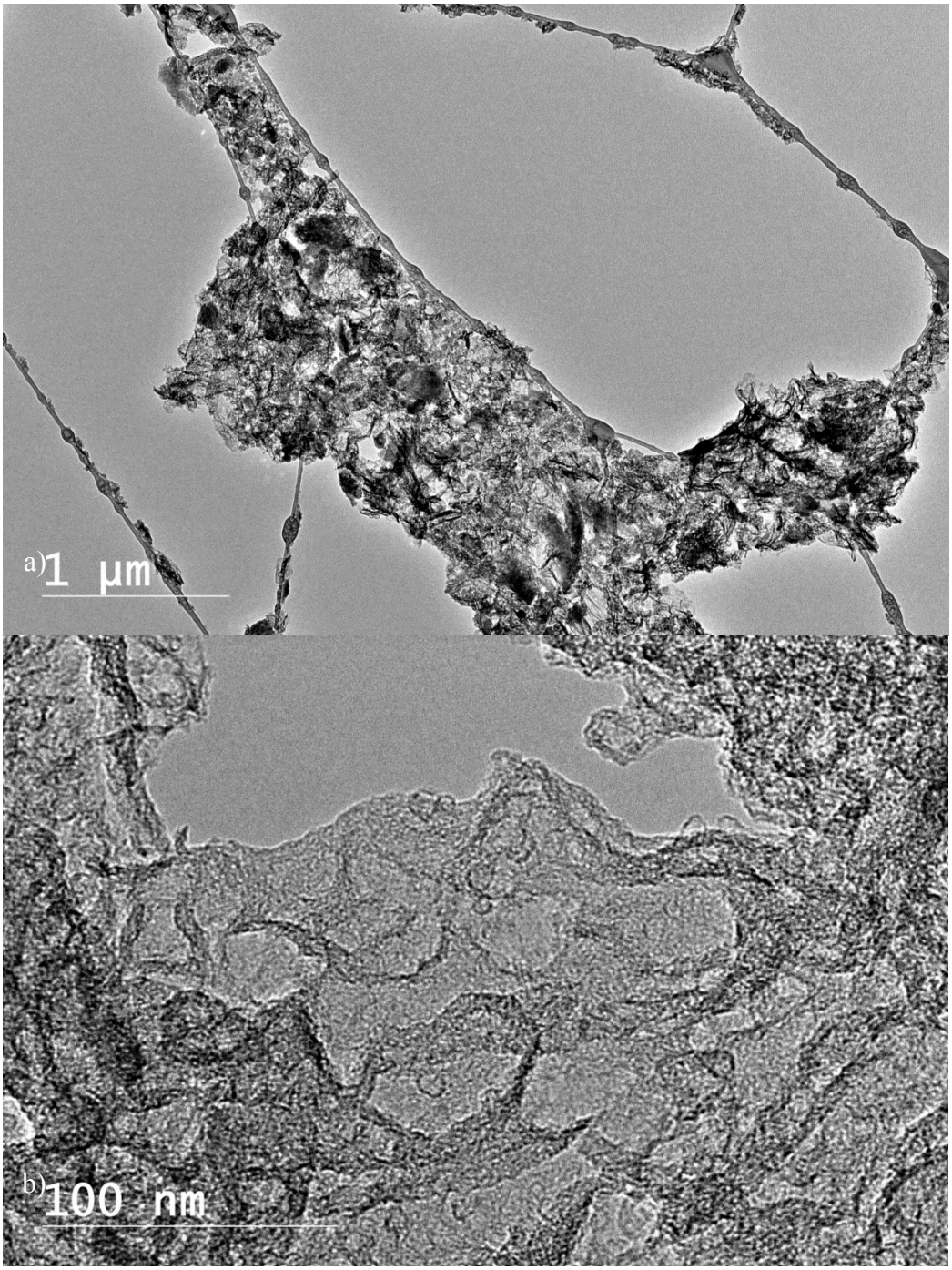

Figure 5.3 TEM images of NMP, PVP functionalized CECNs

5.4 Conclusion

The previously synthesized CECNs were functionalized using NMP and PVP chemicals. FTIR spectrum confirmed the covalent linkages between CECNs and NMP and PVP, indicating a successful functionalization was achieved. The modified CECNs could be dissolved in water and ethanol, and make a homogeneous solution. TEM images demonstrated a uniform dispersion of NMP, PVP functionalized CECNs in the toluene solvent. This study has paved ways for further functionalization of CECNs, making this new product attractive.

5.5 References

Arsalani N, Fattahi H, Nazarpoor M (2010) Synthesis and characterization of PVP-functionalized superparamagnetic Fe3O4 nanoparticles as an MRI contrast agent. Express Polym Lett 4(6): 329-338.

Bissett MA, Takesaki Y, Tsuji M, Ago H (2014) Increased chemical reactivity achieved by asymmetrical 'Janus' functionalisation of graphene. R Soc Chem Adv 4(94): 52215–52219.

Bjerglund E, Kongsfelt M, Shimizu K, Jensen BBE, Koefoed L, Ceccato M, Skrydstrup T, Pedersen SU, Daasbjerg K (2014) Controlled Electrochemical Carboxylation of Graphene To Create a Versatile Chemical Platform for Further Functionalization. Langmuir 30(22): 6622-6628.

Boukhvalov D, Katsnelson M (2008) Chemical Functionalization of Graphene with Defects. Nano Lett 8(12): 4373--4379.

Byun I-S, Kim W, Boukhvalov DW, Hwang I, Son JW, Oh G, Choi JS, Yoon D, Cheong H, Baik J, Shin H-J, Shiu HW, Chen C-H, Son Y-W, Park BH (2014) Electrical control of nanoscale functionalization in graphene by the scanning probe technique. NPG Asia Mater 6(5): e102.

Ebrish MA, Olson EJ, Koester SJ (2014) Effect of Noncovalent Basal Plane Functionalization on the Quantum Capacitance in Graphene. ACS Appl Mater Interf 6(13): 10296-10303.

Ensafi AA, Jafari-Asl M, Rezaei B (2014) A new strategy for the synthesis of 3-D Pt nanoparticles on reduced graphene oxide through surface functionalization, Application for methanol oxidation and oxygen reduction. Electrochim Acta 130: 397-405.

Fernandez-Merino M, Guardia L, Paredes J, Villar-Rodil S, Solis-Fernandez P, Martinez-Alonso A, Tascon J (2010) Vitamin C Is an Ideal Substitute for Hydrazine in theReduction of Graphene Oxide Suspensions. J Phys Chem C 114(14): 6426--6432.

Gardolinski JE, Peralta-Zamora P, Wypych F (1999) Preparation and characterization of a kaolinite-1-methyl-2-pyrrolidone intercalation compound. J Colloid Interf Sci 211(1): 137--141.

Geng Y, Li J, Jing X, Wang F (1997) Interaction of N-methylpyrrolidone with doped polyaniline. Synthetic met 84(1): 97-98.

Giri N, Natarajan R, Gunasekaran S, Shreemathi S (2011) 13C NMR and FTIR spectroscopic study of blend behavior of PVP and nano silver particles. Arch Appl Sci Res 3(5): 624--630.

Hamilton CEaL, Jay R and Sun, Zhengzong and Tour, James M and Barron, Andrew R (2009) High-yield organic dispersions of unfunctionalized graphene. Nano Lett 9(10): 3460--3462.

Jang J, Pham V, Rajagopalan B, Hur S, Chung J (2014) Effects of the alkylamine functionalization of graphene oxide on the properties of polystyrene nanocomposites. Nanoscale Res Lett 9(1): 265.

Jokar E, Iraji Zad A, Shahrokhian S (2014a) Growth control of cobalt oxide nanoparticles on reduced graphene oxide for enhancement of electrochemical capacitance. Int J Hydrogen Energy 39(36): 21068-21075.

Jokar E, Shahrokhian S, Iraji Zad A (2014b) Electrochemical functionalization of graphene nanosheets with catechol derivatives as an effective method for preparation of highly performance supercapacitors. Electrochim Acta 147: 136-142.

Kaur P, Shin M-S, Sharma N, Kaur N, Joshi A, Chae S-R, Park J-S, Kang M-S, Sekhon SS (2015) Non-covalent functionalization of graphene with poly(diallyl dimethylammonium) chloride: Effect of a non-ionic surfactant. Int J Hydrogen Energy 40(3): 1541-1547.

Laot CM, Marand E, Oyama HT (1999) Spectroscopic characterization of molecular interdiffusion at a poly (vinyl pyrrolidone)/vinyl ester interface. Polym 40(5): 1095--1108.

Liu M, Duan Y, Wang Y, Zhao Y (2014) Diazonium functionalization of graphene nanosheets and impact response of aniline modified graphene/bismaleimide nanocomposites. Mater Des 53: 466-474.

Liu J, Wang X, Wang T, Li D, Xi F, Wang J, Wang E (2014) Functionalization of Monolithic and Porous Three-Dimensional Graphene by One-Step Chitosan Electrodeposition for Enzymatic Biosensor. ACS Appl Mater Interf 6(22): 19997-20002.

Nam JA, Nahain A-A, Kim SM, In I, Park SY (2013) Successful stabilization of functionalized hybrid graphene for high-performance antimicrobial activity. Acta Biomater 9(8): 7996-8003.

Nebogatikova NA, Antonova IV, Prinz VY, Volodin VA, Zatsepin DA, Kurmaev EZ, Zhidkov IS, Cholakh SO (2014) Functionalization of graphene and few-layer graphene films in an hydrofluoric acid aqueous solution. Nanotechno in Russia 9(1-2): 51-59.

Nguyen LH, Nguyen TD, Tran VH, Dang TTH, Tran DL (2014) Functionalization of reduced graphene oxide by electroactive polymer for biosensing applications. Advances in Natural Sciences: Nanoscience and Nanotechnology 5(3): 035005.

Roppolo I, Chiappone A, Bejtka K, Celasco E, Chiodoni A, Giorgis F, Sangermano M, Porro S (2014) A powerful tool for graphene functionalization: Benzophenone mediated UV-grafting. Carbon 77: 226-235.

Saravanan L, Diwakar S, Pandurangan A, Jayavel R (2011) Synthesis, Structural and Optical properties of PVP encapsulated CdS nanoparticles. Nanometer Nanotechnol 1(2): 42--48.

Shruthi TK, Ilayaraja N, Jeyakumar D, Sathish M (2014) Functionalization of graphene with nitrogen using ethylenediaminetetraacetic acid and their electrochemical energy storage properties. R Soc Chem Adv 4(46): 24248.

Tu W-x, Zuo X-b, Liu H-f (2008) STUDY ON THE INTERACTION BETWEEN POLYVINYLPYRROLIDONE AND PLATINUM METALS DURING THE FORMATION OF THE COLLOIDAL METAL NANOPARTICLES. Chin J Polym Sci 26(1): 23--29.

Vu TDT, Pham VH, Hur SH, Chung JS (2014) Effect of reduced graphene oxide functionalization by sulfanilic acid on the mechanical properties of poly(styrene-co-acrylonitrile)/reduced graphene oxide composites. Polym Comos.

Wang M, Galpaya D, Lai ZB, Xu Y, Yan C (2014) Surface functionalization on the thermal conductivity of graphene–polymer nanocomposites. Int J Smart Nano Mater 5(2): 123-132.

Wei J, Qiu J (2014) Allyl-Functionalization enhanced thermally stable graphene/fluoroelastomer nanocomposites. Polym 55(16): 3818-3824.

Woszczyna M, Winter A, Grothe M, Willunat A, Wundrack S, Stosch R, Weimann T, Ahlers F, Turchanin A (2014) All-Carbon Vertical van der Waals Heterostructures: Non-destructive Functionalization of Graphene for Electronic Applications. Adv Mater 26(28): 4831-4837.

Xu Z, Wang S, Li Y, Wang M, Shi P, Huang X (2014) Covalent Functionalization of Graphene Oxide with Biocompatible Poly(ethylene glycol) for Delivery of Paclitaxel. ACS Appl Mater Interf 6(19): 17268-17276.

Yi M, Zhang W, Shen Z, Zhang X, Zhao X, Zheng Y, Ma S (2013) Controllable functionalization and wettability transition of graphene-based films by an atomic oxygen strategy. J Nanopart Res 15(8).

Yang L, He J (2014) Organic functionalisation of graphene catalysed by ferric perchlorate. Chem Commun 50(99): 15722--15725.

Zhang X, Hsu A, Wang H, Song Y, Kong J, Dresselhaus MS, Palacios T (2013) Impact of Chlorine Functionalization on High-Mobility Chemical Vapor Deposition Grown Graphene. ACS nano 7(8): 7262--7270.

CHAPTER VI

CONCLUSION AND FUTURE WORK

6.1 Conclusion

In this project, the possibility of synthesize CECNs using lignin, beetle-killed tree, and copper sulfate as the raw material was systematically studied. The synthesis mechanism was proposed. In addition, the process parameters were optimized. Finally, the CECNs was functionalized in order to broad their application. During the research, we have learned and observed some interesting results.

1) In the preliminary study, the hypothesis that CECNs be synthesized using simple thermal treatment with sustainable bioproducts and copper sulfate pentahydrate as the raw material were inspected. Beetle-killed tree was tried and failed, with no signs of graphene layers being observed. While BCL-DI lignin was proved to be a success. CECNs were successfully synthesized at 1000 ºC, 1h duration time, 20 ºC/min, and 1800 sccm argon gas flow rate. Samples were analyzed by X-ray diffraction, SEM, and TEM microscopy. The yield of graphene was limited. CECNs were mainly located at defect sites. Copper was found not tightly encapsulated by graphene shells. The CECNs were uniformly distributed. Crystallinity of carbon material was low, and amorphous carbon needs to be removed or converted into crystalline carbon.

2) The graphene forming process and changes of copper valence were investigated from 200 ºC to 500 ºC. Abrupt conversion of copper ions into copper atoms occurred at above 300 ºC, with the company of decomposition of BCL-DI lignin into CO, CO_2, and hydrocarbon gases. The growth of graphene layers was proposed to start above 300 ºC. TEM images illustrated the start of growth of graphene at the edge of the surface at 400 ºC, and the formation of graphene bands at 500 ºC.
3) The effect of copper catalyst on the synthesis of CECNs was studied from 600 ºC to 1000 ºC. Copper catalyst facilitated the decomposition of lignin functional groups at 600 ºC. Further increasing the temperature retarded the degradation of lignin, while assisted the reconstruction of the defective sites of the graphene layers, producing higher quality products. It was proposed that plastic lignin film dominated the synthesis of CECNs, while gaseous phase had little impact on the growth of CECNs, might be due to the experiment setup.
4) The $L_9(3^4)$ orthogonal experiment was designed to find out the optimum process parameters to synthesize high quality CECNs. Temperature played the most important role in the growth of graphene: high temperature was preferred in order to obtain less defective sites. Complicate reactions existed during the annealing process. The optimum synthesis parameters were suggested as 1000 °C, 30 min duration time, 20 °C/min temperature rising ramp, and 1200 sccm argon gas flow rate.

5) Post heat treatment was proved to be a feasible way to improve the crystallinity of graphite. Amorphous carbon was removed or converted into crystalline graphite under heat and oxygen.
6) As for the functionalization of CECNs with NMP and PVP chemicals in order to make a homogeneous solution, FTIR spectra confirmed the covalent linkages between CECNs and NMP and PVP, indicating a successful functionalization. TEM images illustrated uniform dispersion of NMP, PVP functionalized CECNs in the toluene solvent. This study has produced a homogeneous CECNs solution in water and ethanol, and paved ways for further functionalization of CECNs.

6.2 Future work

In future study, focus should be put on the increase of CECNs yield, and the extraction of pure CECNS or pure graphene layers, depending on the specific application. Scale up is another field needs specific attention since large amount of lignin is available in bioproducts industry. Kilograms of CECNs should be produced with consistent quality. Another focus should be on the functionalization of CECNs with more kinds of chemicals, and create novel products.

6.3 References

Balandin AA, Ghosh S, Bao W, Calizo I, Teweldebrhan D, Miao F, Lau CN (2008) Superior Thermal Conductivity of Single-Layer Graphene. Nano Lett 8(3): 902--907.

Bokhonov BB, Novopashin SA (2010) In situ investigation of morphological and phase changes during thermal annealing and oxidation of carbon-encapsulated copper nanoparticles. J Nanopart Res 12(8): 2771-2777.

Bolotin KI, Sikes KJ, Jiang Z, Klima M, Fudenberg G, Hone J, Kim P, Stormer HL (2008) Ultrahigh electron mobility in suspended graphene. Solid State Commun 146(9-10): 351-355.

El-Gendy AA, Ibrahim EMM, Khavrus VO, Krupskaya Y, Hampel S, Leonhardt A, Büchner B, Klingeler R (2009) The synthesis of carbon coated Fe, Co and Ni nanoparticles and an examination of their magnetic properties. Carbon 47(12): 2821-2828.

Fisher AB, Fong SS (2014) Lignin biodegradation and industrial implications AIMS Bioeng 1(2): 92-112.

Gómez-Navarro C, Burghard M, Kern K (2008) Elastic Properties of Chemically Derived Single Graphene Sheets. Nano Lett 8(7): 2045-2049.

Guo F, Shi W, Sun W, Li X, Wang F, Zhao J, Qu Y (2014) Differences in the adsorption of enzymes onto lignins from diverse types of lignocellulosic biomass and the underlying mechanism. Biotechnol Biofuels 7(1): 38.

Jeong N, Han SO, Kim H, Kim H-s, You Y-j (2010) Growth of multi-walled carbon nanotubes by catalytic decomposition of acetylene on Ni-supported carbon fibers prepared by the heat-treatment of cellulose fibers. J Mater Sci 46(7): 2041-2049.

Karmakar A, Xu Y, Mahmood MW, Zhang Y, Saeed LM, Mustafa T, Ali S, Biris AR, Biris AS (2011) Radio-frequency induced in vitro thermal ablation of cancer cells by EGF functionalized carbon-coated magnetic nanoparticles. J Mater Chem 21(34): 12761.

Khenfouch M, Buttner U, Baïtoul M, Maaza M (2014) Synthesis and Characterization of Mass Produced High Quality Few Layered Graphene Sheets via a Chemical Method. Graphene 03(02): 7-13.

Kuila T, Bose S, Mishra AK, Khanra P, Kim NH, Lee JH (2012) Chemical functionalization of graphene and its applications. Prog Mater Sci 57(7): 1061-1105.

Kuznetsov V, Usoltseva A, Chuvilin A, Obraztsova E, Bonard J-M (2001) Thermodynamic analysis of nucleation of carbon deposits on metal particles and its implications for the growth of carbon nanotubes. Phys Rev B 64(23).

Lamastra FR, Puglia D, Monti M, Vella A, Peponi L, Kenny JM, Nanni F (2012) Poly(ε-caprolactone) reinforced with fibres of Poly(methyl methacrylate) loaded with multiwall carbon nanotubes or graphene nanoplatelets. Chem Eng J 195-196: 140-148.

Laude T, Kuwahara H, Sato K (2007) FeCl2-CVD production of carbon fibres with graphene layers nearly perpendicular to axis. Chem Phys Lett 434(1-3): 78-81.

Lee C, Wei X, Kysar JW, Hone J (2008) Measurement of the Elastic Properties and Intrinsic Strength of Monolayer Graphene. Sci 321(5887): 385-388.

Li C, Li D, Yang J, Zeng X, Yuan W (2011) Preparation of Single- and Few-Layer Graphene Sheets Using Co Deposition on SiC Substrate. J Nanomater 2011: 1-7.

Liu N, Fu L, Dai B, Yan K, Liu X, Zhao R, Zhang Y, Liu Z (2011) Universal Segregation Growth Approach to Wafer-Size Graphene from Non-Noble Metals. Nano Lett 11(1): 297-303.

Loh KP, Bao Q, Ang PK, Yang J (2010) The chemistry of graphene. J Mater Chem 20(12): 2277.

Mbuyisa P, Bhardwaj SP, Rigoni F, Carlino E, Pagliara S, Sangaletti L, Goldoni A, Ndwandwe M, Cepek C (2012) Controlled synthesis of carbon nanostructures using aligned ZnO nanorods as templates. Carbon 50(15): 5472-5480.

Meng L, Sun Q, Wang J, Ding F (2012) Molecular Dynamics Simulation of Chemical Vapor Deposition Graphene Growth on Ni (111) Surface. J Phys Chem C 116(10): 6097-6102.

Mody VV, Siwale R, Singh A, Mody HR (2010) Introduction to metallic nanoparticles. J Pharm Bioall Sci 2(4): 282-289.

Morozov S, Novoselov K, Katsnelson M, Schedin F, Elias D, Jaszczak J, Geim A (2008) Giant Intrinsic Carrier Mobilities in Graphene and Its Bilayer. Phys Rev Lett 100(1).

Motozuka S, Tagaya M, Ikoma T, Yoshioka T, Xu Z, Tanaka J (2012) Preparation of copper-graphite composite particles by milling process. J Compos Mater 46(22): 2829-2834.

Mwakikunga BW, Hillie KT. (2011). Graphene synthesis, catalysis with transition metals and their interactions by laser photolysis. In Gong J (Ed.) Graphene synthesis, characterization, properties and applications. Intech.

Norimatsu W, Kusunoki M (2010) Formation process of graphene on SiC (0001). Physica E Low Dimens Syst Nanostruct 42(4): 691-694.

Obare SO, Meyer GJ (2004) Nanostructured Materials for Environmental Remediation of Organic Contaminants in Water. J Environ Sci Health A Tox Hazard Subst Environ Eng 39(10): 2549-2582.

Popławska M, Żukowska GZ, Cudziło S, Bystrzejewski M (2010) Chemical functionalization of carbon-encapsulated magnetic nanoparticles by 1,3-dipolar cycloaddition of nitrile oxide. Carbon 48(4): 1318-1320.

Ramón ME, Gupta A, Corbet C, Ferrer DA, Movva HC, Carpenter G, Banerjee SK (2011) CMOS-Compatible Synthesis of large-area, high-mobility graphene by chemical vapor deposition of acetylene on cobalt thin films. ACS nano 5(9): 7198-7204.

Sjöström E. (1993). Wood Chemistry: Fundamentals and Application. Acdamic Press: Gulf Professional Publishing. 293 pp.

Song H, Chen X (2003) Large-scale synthesis of carbon-encapsulated iron carbide nanoparticles by co-carbonization of durene with ferrocene. Chem Phys Lett 374(3-4): 400-404.

Sun Z, Raji A-RO, Zhu Y, Xiang C, Yan Z, Kittrell C, Samuel E, Tour JM (2012) Large-Area Bernal-Stacked Bi-, Tri-, and Tetralayer Graphene. ACS nano 6(11): 9790--9796.

Taylor A, Krupskaya Y, Costa S, Oswald S, Krämer K, Füssel S, Klingeler R, Büchner B, Borowiak-Palen E, Wirth MP (2009) Functionalization of carbon encapsulated iron nanoparticles. J Nanopart Res 12(2): 513-519.

Tessonnier J-P, Rosenthal D, Hansen TW, Hess C, Schuster ME, Blume R, Girgsdies F, Pfänder N, Timpe O, Su DS, Schlögl R (2009) Analysis of the structure and chemical properties of some commercial carbon nanostructures. Carbon 47(7): 1779-1798.

Wang S, Huang X, He Y, Huang H, Wu Y, Hou L, Liu X, Yang T, Zou J, Huang B (2012) Synthesis, growth mechanism and thermal stability of copper nanoparticles encapsulated by multi-layer graphene. Carbon 50(6): 2119-2125.

Weisenberger M, Martin-Gullon I, Vera-Agullo J, Varela-Rizo H, Merino C, Andrews R, Qian D, Rantell T (2009) The effect of graphitization temperature on the structure of helical-ribbon carbon nanofibers. Carbon 47(9): 2211-2218.

Zan W (2014) Chemical functionalization of graphene by carbene cycloaddition: A density functional theory study. Appl Surf Sci 311: 377-383.

Zhang G, Sun S, Yang D, Dodelet J-P, Sacher E (2008) The surface analytical characterization of carbon fibers functionalized by H2SO4/HNO3 treatment. Carbon 46(2): 196-205.

Zhu Y, Murali S, Cai W, Li X, Suk JW, Potts JR, Ruoff RS (2010) Graphene and Graphene Oxide: Synthesis, Properties, and Applications. Adv Mater 22(35): 3906-3924.

Zou Z, Dai B, Liu Z (2013) CVD process engineering for designed growth of graphene. Sci Sin Chim 43(1): 1.